CONTENTS A THROUGH E

ALKALI METALS IN THE CORE? EXPERIMENTAL CONSTRAINTS ON MAGMA OCEAN PARTITIONING OF CS, K, AND NA. C. B. Agee, N. M. Mills, D. S. Draper, Astromaterials Institute, University of New Mexico, Albuquerque, NM 87131, agee@unm.edu.

Introduction: In earlier work, it was demonstrated that refractory lithophile elements vanadium (V) and chromium (Cr) become slightly siderophile at very high temperatures and at low oxygen fugacities (Chabot and Agee, 2003 [1]). Thus mantle depletions in V and Cr (figure 1) are consistent with sequestering a significant amount of these elements in the core during a magma ocean stage of early Earth differentiation.

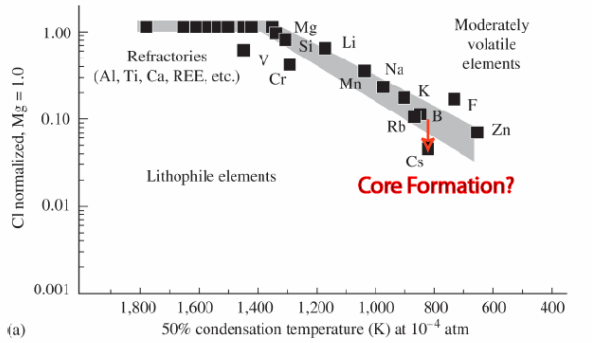

Figure 1. From Palme and O'Neill (2004) [2] showing the CI normalized abundance of some lithophile elements in the silicate Earth.

We now focus our experimental studies on cesium (Cs) which also shows an apparent depletion in the silicate Earth. A complicating factor here is that Cs, like the other volatile elements, is depleted in the bulk Earth relative to chondrites due to accretion processes. This depletion of lithophile, volatile elements is shown in figure 1 and is often referred to as the "volatility trend". A notable feature of the volatility trend is that Cs actually falls below the trend, thus it is relatively more depleted than the other volatile elements shown. This depletion could indicate that there is some unaccounted-for, accreted Cs that is sequestered in a reservoir other than the sampled silicate Earth – one possible reservoir being the Earth's core. McDonough (2004) [3] estimates that this depletion would be equivalent to 55-60% of the Earth's Cs residing in the core, with a metal/silicate enrichment factor of about three. Indeed, there have been several recent studies on alkali metals, with much attention focused on potassium (K), that support the hypothesis that these elements can become slightly siderophile, either through compositional effects (Murthy et al., 2003) [4] or by pressure induced electronic transitions (Lee et al., 2004) [5]. Of the alkali metals, Cs shows the most pronounced depletion deviation from the volatility trend, and therefore one could argue that it is the most likely of these elements to show slightly siderophile behavior during conditions of core formation. For this reason, we believe Cs partitioning studies between metal and silicate should have the highest likelihood of the alkali metals to reveal slightly siderophile behavior and should have experimental priority. To this end we have initiated a study to scope out the P-T-X conditions under which Cs D-metal/silicate values can approach unity or higher. We also present here data on partitioning of K and Na in order to elucidate systematics of the other alkali metals at high pressures, high temperatures, variable nbo/t, and sulfur content. Potassium partitioning between metal and silicate, and the possibility of K in the core have received much attention recently. However, to our knowledge, there are no studies that have examined the alkali metals as a group. There is some indication that the heavy alkali metals such as Rb and Cs will show the 4s to 3d electronic transition at lower pressures than Li, Na, and K. If so, then variable mantle depletions and core enrichments of light alkali metals versus heavy alkali metals could potentially be used as geobarometer for the depth of planetary core formation.

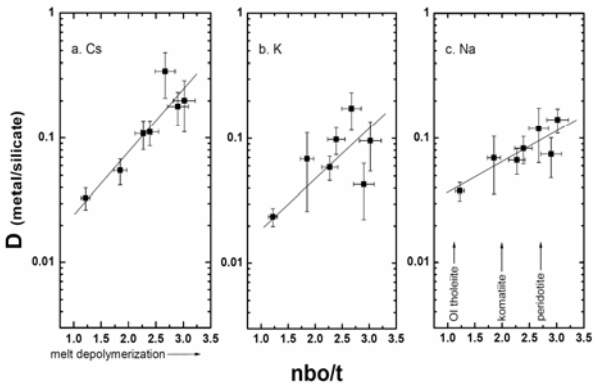

Figure 2. Variation in metal-silicate partition coefficient with melt polymerization at 5 GPa and 2100 for (a) Cs, (b) K, and (c) Na. The correlation of Cs measurements was significantly better than for the other alkalis. It appears that Cs is the most responsive to changes in melt polymerization, and that the degree of change is related to the size of the alkali elements.

Experimental: Experiments were carried out in the Astromaterials High Pressure Laboratory at the University of New Mexico, using a Walker-style multi-anvil device. We ran several series of experiments where P-T-X-fO2-S-nbo/t were varied independently in order to isolate the various effects on element partitioning. The pressure range was from 5-

15 GPa, temperature from 1900-2400°C, metallic sulfur content from pure Fe to pure FeS, silicate nbo/t from 1.26 to 3.1, and oxygen fugacity from two to four log units below the iron-wustite buffer. Silicate melt composition (nbo/t) and sulfur content of the molten Fe-alloy were the two variables that influenced alkali metal partitioning the greatest. Figure 2 shows that Cs partitioning between metal and silicate strongly increases with silicate melt de-polymerization, with K and Na showing more modest increases. Figure 3 shows that D metal/silicate increases dramatically for the alkali metals at sulfur contents of about 25 wt%.

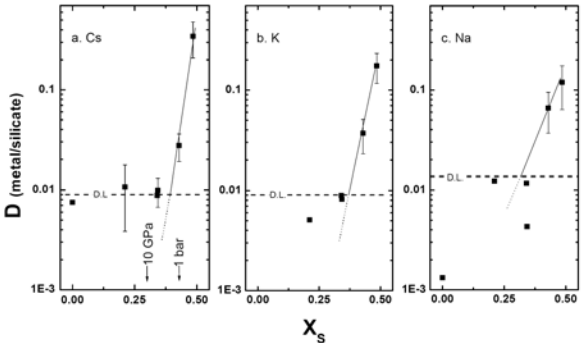

Figure 3. Variation in metal-silicate partition coefficient with S content for (a) Cs, (b) K, and (c) Na. The majority of experiments below about 25 wt% S in the metal phase yielded analyses that were below detection limits for each element. Above 25 wt%, D-values rise significantly, with the larger alkali elements tending to be more responsive than the smaller ones. Error bars are +/- 1σ, and error bars from analyses below detection limits are not shown. The Fe-FeS eutectic composition (Fei et al. 1997) is indicated at 1 bar and 10 GPa.

Temperature showed a weak positive effect on D and we observed no pressure effect on D for the alkali metals between 5 and 15 GPa.

Discussion: Under the conditions of our experiments we observe marked increase in D metal/silicate for Cs, K, and Na with de-polymerization of the silicate melt and sulfur content of the metal. Cs shows the largest increases in D of the three alkali metals investigated with a maximum D-value of 0.345 (0.175 for K and 0.119 for Na) in a sulfur-rich, peridotitic system at 5 GPa and 2100°C. For example, these experimental Ds, if applied to a magma ocean scenario, would partition 14.2%, 7.7%, and 5.4% of the bulk Earth's Cs, K, and Na into the core. Our experiments indicate that under certain conditions Cs is approaching "slightly" siderophile behavior, however it is still significantly lower than the D-value required to account for all of the observed mantle Cs depletion through core formation (D~2-3).

We believe that further experimentation is warranted, especially at pressures above 15 GPa. Because silicate melt structure effects D, it is important to carry out experiments at lower mantle pressures where silicon is closer packed and octahedrally coordinated with oxygen. Another motivation for exploring higher experimental pressures is that we have not yet observed the s-orbital to d-orbital transition predicted by Bukowinski (1976) [7]. This shift should cause alkali metals to behave more like transition metals, which also have electrons in *d* orbitals, and thus display a drastically increased solubility in iron, and a discontinuous change in D metal-silicate at some high pressure threshold.

References:

[1] Chabot N.L. and Agee C.B. (2003) *GCA, 67,* 2077-2091. [2] Palme H. and O'Neill H. St. C. (2004) *Treatise on Geochemisry, 2*, 1-38. [3] McDonough W. F. (2004) *Treatise on Geochemisry*, 2, 547-568. [4] Murthy R. M., van Westrenen W., and Fei Y. (2003) *Nature 423*, 163-165. [5] Lee K. K. M., Steinle-Neumann G., and Jeanloz R. (2004) *GRL, 31,* GL019839. [6] Bukowinski M. S. T. (1976) *GRL, 3*, 491-494.

GIANT IMPACTS AND TERRESTRIAL PLANET EVOLUTION. Craig B. Agnor and Erik Asphaug, *CODEP, Department of Earth & Planetary Sciences, University of California, Santa Cruz, CA 95064 (Email: cagnor@es.ucsc.edu).*

The terrestrial planets are generally thought to have formed via the collisional accumulation of smaller rocky bodies. As such, collisions represent an important evolutionary process, one that plays a significant role in determining the final characteristics of the planets (e.g. thermal evolution and associated differentiation, rotation states, composition). Here we will examine the frequency and nature of giant impacts (i.e. collisions between $\sim 10^3$km planetary embryos of similar size) during planet formation, present model results of these collisions, relate collision outcomes to different modes of planetary accretion and discuss the implications of these giant collisions for the evolution of the terrestrial planets.

Dynamical modeling of terrestrial planet accretion is typically divided into several separate regimes according to the dominant modes of growth: (A) the formation of ∼km-sized planetesimals; (B) the runaway and oligarchic accumulation of planetesimals into $\sim 10^3$km planetary embryos; and (C) the late stage where continued planetary accretion requires collisions between embryos and the sweep up of any remaining planetesimals.

Recent work has elucidated many of the aspects related to the transition between rapid runaway and the more gradual oligarchic growth of planetary embryos [e.g. 1, 2, 3]. Through the accumulation of smaller planetesimals, embryos' feeding zones expand and begin to overlap. As this occurs the embryos (or 'battling oligarchs') will suffer close encounters and collisions [3]. Thus, giant impacts between embryos of comparable mass are an integral part of accretion during the earlier stage of runaway and oligarchic growth (B) when the total mass in embryos may be small relative to the total mass of the swarm of planetesimals, as well as the later (stage C) when planetary embryos may dominate the mass distribution.

Studies of planet formation and planetary collisional evolution have typically been conducted separately. Most dynamical studies of planet formation employ inelastic mergers as a simplifying model assumption [e.g. 4, 5, 6, 7]. On the other hand, most of the work studying the collisional evolution of terrestrial planets has focused on determining the ability of single impacts to account for particular planetary characteristics or the formation of satellites [e.g. 8, 9, 10].

We are using a smoothed particle hydrodynamics (SPH) code [e.g. 11] to model giant impacts between planetary embryos of the type prevalent during terrestrial planet accumulation. Our efforts are focused on characterizing the outcomes of the collisions and evaluating the geophysical processing of the colliding embryos and growing planets. In addition to the well studied aspects of mantle stripping via head-on, high velocity impacts [8] and satellite formation through low-velocity glancing blows [e.g. 12, 10], our simulation results clearly demonstrate that for conditions common during terrestrial planet accretion, collisions between planetary embryos may have a variety of bulk outcomes including: merger or rebound of embryos (i.e. 'hit-and-run' collisions), and erosion varying in degree from slight mass lost to shearing into several smaller embryos to complete destruction of the an embryo into much smaller debris [13, 14].

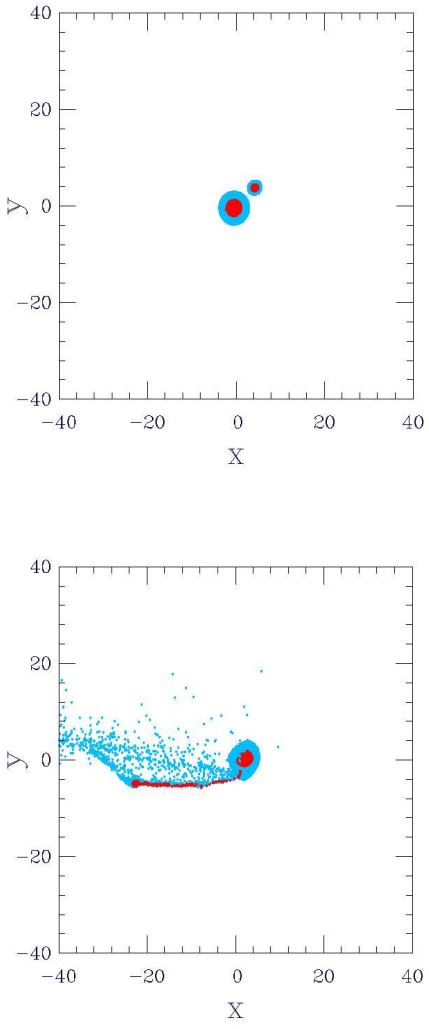

Figure 1: **Simulation results from a typical 'hit-and-run' collision.** Two snapshots just before (top) and a few hours after (bottom) an impact between a $M_T = 0.10M_\oplus$ target and an impactor of mass $M_I = 0.01M_\oplus$. We used the Tillotson equation of state with basalt (shown with blue/light particles) and iron (shown with red/dark particles) material parameters to model the mantle and core respectively. The two bodies collide with a velocity fifty-percent greater than their mutual escape velocity with an impact angle of $\xi = 45°$.

Placing these model results in the context of planetary formation models it is apparent that the material ultimately incorporated into the planets may have suffered multiple giant impacts, many of which were catastrophic thermodynamical events and/or were non-accretionary rebound or disruptive impacts. In this presentation we will discuss the connection between the style of accretion (e.g. oligarchic vs. late stage), impact dynamics and collision outcomes as well as their implication for the thermal, rotational and compositional evolution of the terrestrial planets.

This research has been supported by NASA's PG&G and Origins programs.

[1] E. Kokubo and S. Ida. Oligarchic growth of protoplanets. *Icarus*, 131:171–178, January 1998.

[2] E. W. Thommes, M. J. Duncan, and H. F. Levison. Oligarchic growth of giant planets. *Icarus*, 161:431–455, February 2003.

[3] P. Goldreich, Y. Lithwick, and R. Sari. Planet Formation by Coagulation: A Focus on Uranus and Neptune. *ARA&A*, 42:549–601, September 2004.

[4] C. B. Agnor, R. M. Canup, and H. F. Levison. On the character and consequences of large impacts in the late stage of terrestrial planet formation. *Icarus*, 142:219–237, November 1999.

[5] J. E. Chambers. Making more terrestrial planets. *Icarus*, 152:205–224, August 2001.

[6] H. F. Levison and C. Agnor. The role of giant planets in terrestrial planet formation. *AJ*, 125:2692–2713, May 2003.

[7] S. N. Raymond, T. Quinn, and J. I. Lunine. Making other earths: dynamical simulations of terrestrial planet formation and water delivery. *Icarus*, 168:1–17, March 2004.

[8] W. Benz, W. L. Slattery, and A. G. W. Cameron. Collisional stripping of Mercury's mantle. *Icarus*, 74:516–528, June 1988.

[9] R. M. Canup and E. Asphaug. Origin of the Moon in a giant impact near the end of the Earth's formation. *Nature*, 412:708–712, August 2001.

[10] R. M. Canup. Simulations of a late lunar-forming impact. *Icarus*, 168:433–456, April 2004.

[11] W. Benz. Smooth Particle Hydrodynamics - a Review. In J. R. Buchler, editor, *Numerical Modelling of Nonlinear Stellar Pulsations Problems and Prospects*, pages 269–288, 1990.

[12] W. Benz, A. G. W. Cameron, and H. J. Melosh. The origin of the Moon and the single impact hypothesis. III. *Icarus*, 81:113–131, September 1989.

[13] C. Agnor and E. Asphaug. Accretion Efficiency during Planetary Collisions. *ApJ*, 613:L157–L160, October 2004.

[14] E. Asphaug, C. B. Agnor, and Q. Williams. Hit-and-run planetary collisions. *Nature*, 439:155–160, January 2006.

THREE-STAGE EPISODIC EARTH EVOLUTION. Nicholas Arndt[1] and Anne Davaillé[2], [1] LGCA, University of Grenoble, 38400 Grenoble, France <arndt@ujf-grenoble.fr>, [2] IPGP, 4 place Jussieu, Paris, France

U-Pb ages of zircons in granites and large rivers record a three-stage evolution of the continental crust. Plate tectonics operated in the first stage, from ~4.4 to 2.7 Ga. Huge peaks of crustal growth separated by long troughs dominated the second stage, from 2.7 to 1.8 Ga. Semi-continuous growth punctuated by large peaks characterized the last stage, from 1.8 to O Ga. Individual peaks in the second stage open with massive mafic-ultramafic volcanism and climax 30 m.y. later with intrusion of voluminous granitoids: each peak opened with enhanced mantle plume activity, climaxed with accelerated plate tectonic activity, and was followed by a long quiet period when little crust formed. We develop a fluid-mechanics model to explain the three-stage evolution and the pronounced peak-and-trough pattern of the second stage. Low temperatures in the mantle during the first and last stages allowed the formation of thin, subductable oceanic crust and led to a plate-tectonic regime. The crustal-growth peaks of the second regime resulted from destabilization of a hot lower-mantle layer. Domes rising from this layer partially melted to form voluminous mafic magmas; they also heated the upper mantle, initially accelerating crustal growth but then forming thick unsubductable crust that temporally choked off plate tectonics.

PARTITIONING OF OXYGEN BETWEEN MAGNESIOWÜSTITE AND LIQUID IRON: CONSEQUENCES FOR THE EARLY DIFFERENTIATION OF TERRESTRIAL PLANETS. Y. Asahara[1], D. C. Rubie[1] and D. J. Frost[1], [1]Bayerisches Geoinstitut; Universität Bayreuth, D-95440 Bayreuth, Germany, Dave.Rubie@uni-bayreuth.de.

Introduction: The partitioning of oxygen between silicates and liquid Fe-rich metallic alloy is a key factor in controlling chemical differentiation during core formation in terrestrial planets [1]. This is because oxygen partitioning determines the oxygen fugacity uniquely for a given bulk composition and therefore controls the partitioning of Fe and other siderophile elements during core formation.

Although oxygen was proposed many years ago to be a possible light element in the Earth's core, the effect of pressure on oxygen solubility in liquid iron has been controversial. Based on phase relations in the Fe-FeO system, oxygen solubility in liquid Fe increases with increasing pressure. However, according to previous results on the partitioning of oxygen between magnesiowüstite and liquid iron, oxygen solubility in liquid iron has been shown to decrease with increasing pressure [1,2]. Here we report new data on oxygen partitioning between magnesiowüstite and liquid iron in the Fe-FeO-MgO system, obtained over a wide *P-T* range (3-25 GPa, 2273-3173 K), which resolve this issue.

Experimental procedure: Experiments were performed at high pressures and temperatures using a Kawai-type multi-anvil apparatus. Starting materials were mixtures of Fe metal and Fe_2O_3 oxide powders with a range of bulk oxygen contents. We used cylindrical capsules machined from MgO single crystals as sample containers. Chemical analysis and image analysis of recovered samples were carried out using electron microprobe analysis and scanning electron microscopy respectively.

Results: Oxygen contents in the quenched liquid Fe range up to 7.5 wt%. In order to analyze the data, we consider the following reaction of oxygen between magnesiowüstite and Fe liquid:

$$FeO^{\text{magnesiowüstite}} = Fe^{\text{metal}} + O^{\text{metal}} \qquad (1).$$

The distribution coefficient, K_d, for this reaction is independent of oxygen fugacity and is given by

$$K_d = X^{met}_{O} X^{met}_{Fe} / X^{mw}_{FeO}$$

where X^{met}_{O}, X^{met}_{Fe}, X^{mw}_{FeO} are the mol fractions of oxygen in metal, Fe in metal and FeO in magnesiowüstite, respectively. $\ln K_d$ increases with increasing temperature over the range of experimental conditions and shows a linear relationship with $1/T$ at 15-24.5 GPa, and 2273-3173 K. The effect of pressure on $\ln K_d$ is weak up to 25 GPa but $\ln K_d$ appears to initially decrease with increasing pressure, reach a minimum at 10-15 GPa and then increase at higher pressures (Fig. 1). This behavior is caused by the volume change (ΔV) of reaction (1) being pressure-dependent and changing from being positive at <10 GPa to negative at >15 GPa. The change in ΔV is the result the FeO component being more compressible in liquid Fe than in magnesiowüstite.

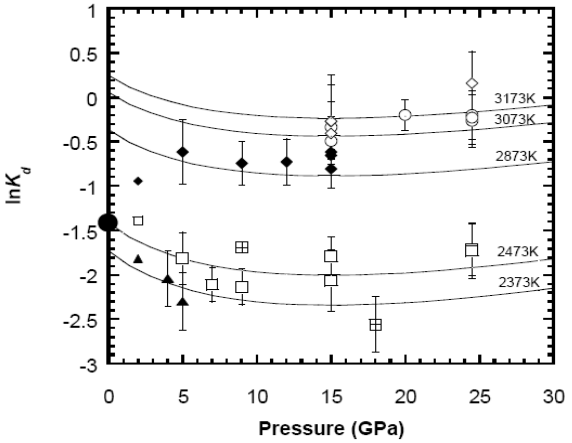

Fig. 1. Relation between $\ln K_d$ and pressure up to 25 GPa. Data from this study: filled triangles: 2373 K; open squares: 2473 K; filled diamonds: 2873 K; open circles: 3073 K; open diamonds: 3150 K. Data from Ohtani and Ringwood [3] at 2 GPa: small filled triangle: 2373 K; small open square: 2473 K; small filled diamond: 2823 K. Squares with crosses: calculated $\ln K_d$ at 2473K based on the data from [1,2]. Large filled circle: $\ln K_d$ at 1 bar and 2473 K calculated using an associated solution model for the Fe-O system. The model discussed below is shown by the fitted lines.

The new experimental data, together with data from Takafuji et al. [4] obtained using a laser-heated diamond anvil cell up to 97 GPa and 3150 K, have been fitted by the equation:

$$RT\ln K_d = -\Delta H + T\Delta S - \int \Delta V dP$$

where ΔH, ΔS and ΔV are the changes in enthalpy, entropy and volume, respectively, for the oxygen exchange reaction (1) and R is the gas constant. Activity coefficients of oxygen in metal, Fe in metal and FeO in magnesiowüstite were assumed to be unity. To evaluate $\int \Delta V dP$, we used an equation of state for the FeO component in liquid Fe that, together with a previously-determined equation of state of wüstite, is consistent with the observed pressure dependence of $\ln K_d$. Obtained parameters for the equation of state of the FeO component in liquid Fe are: $V_{0,\ 298K}$ = 14.7 cm^3/mol, K_0 = 18.6 GPa and K' = 8.5. The values ΔH

$= 1.55 \times 10^5$ J/mol and $\Delta S = 51$ J/K/mol are obtained from the fit. The resulting model reproduces well the entire data set, as shown in Figs. 1 and 2.

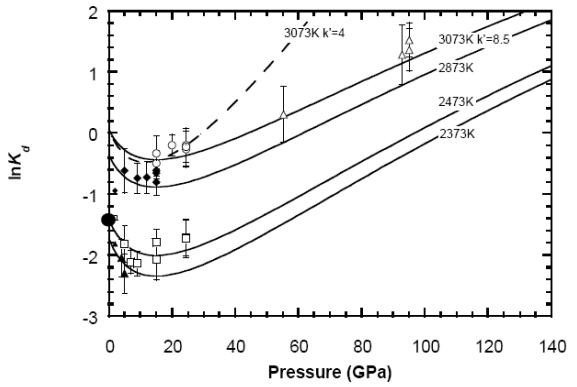

Fig. 2. Relation between lnK_d and pressure up to 140 GPa. Open triangles show calculated lnK_d values based on data obtained at 3000-3150 K by Takafuji et al. [4]. Because only silicate perovskite coexisted with liquid Fe in their experiments, we used the Mg-Fe partition coefficient between magnesiowüstite and Mg-perovskite [5] to estimate the composition of coexisting magnesiowüstite for the determination of K_d. Other symbols are the same as in Fig. 1.

This new model resolves the earlier controversy over the effect of pressure on oxygen solubility in liquid Fe: at constant temperature, solubility decreases with increasing pressure at low pressures but increases with increasing pressure above 15 GPa.

Core Formation Model: We consider the consequences of the dependence of oxygen partitioning between liquid Fe and silicate liquid on P and T for core formation following the model of [1]. We assume that the temperature at the base of the magma ocean is defined by the peridotite solidus [6], and, for simplicity, that the conditions of equilibration between metallic liquid and silicate liquid are approximately those at the base of the magma ocean. We assume a model primitive bulk composition for Earth and Mars which has the major elements Si, Al, Mg, Fe, and Ca in carbonaceous chondritic proportions with some proportion of the total Fe being in the reduced metallic state. Three different initial oxidation states are considered, in which the initial FeO content of the silicate fraction has values of 10, 18 and 25 wt%. The intermediate FeO content is similar to that of the current Martian mantle. The results are shown in Fig 3. In the case of the Earth, the oxygen concentration in liquid Fe in the magma ocean increases with increasing depth and, consequently, the FeO concentration in the residual silicate melt decreases (Fig. 3a). At a magma ocean depth of 1000-1500 km (40-60 GPa), the FeO content of the silicate liquid is reduced to about 8 wt.%, which is comparable to the FeO concentration of Earth's mantle. Depending on the initial oxidation state, up to 8 wt% oxygen is contained in the Earth's core, which is consistent with theoretical predictions [7]. In the case of Mars, because pressures and temperatures are relatively low in a Martian magma ocean, oxygen solubility in liquid Fe is low, independent of magma ocean depth. Core formation thus has little effect on the FeO content of the silicate fraction (Fig. 3b) and the oxygen content of the Martian core is predicted to be low (<3wt%). The model also explains the different mass fractions of the cores of Earth (~30% of the total planet) and Mars (~20%) because more metal segregates from the magma ocean on Earth than on Mars.

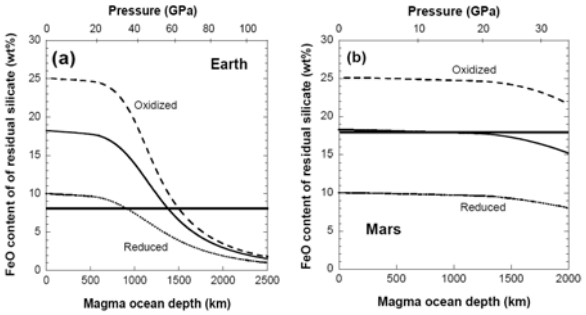

Fig. 3. Results of the core-formation model. The FeO content (wt%) of the residual silicate mantle, as a function of magma ocean depth, is shown for Earth (a) and Mars (b). The three curves show results for starting compositions with different oxygen contents: in the most oxidised composition (dashed line, "oxidised"), the initial FeO content of the silicate fraction was 25 wt% and 40% of the Fe was present as reduced metal; in the intermediate composition (solid line), the initial FeO content of the silicate fraction was ~18 wt% and 60% of the Fe was present as reduced metal; in the most reduced composition (dotted line, "reduced"), the initial FeO content of the silicate fraction was 10 wt% and 80% of the Fe was present as reduced metal. The horizontal lines show the present FeO contents of the mantles of Earth and Mars. For the intermediate starting composition, a magma ocean 1400 km deep would result in the present FeO content of the Earth's mantle and ~8 wt% O in the core. In the case of Mars, the intermediate starting composition results in the current FeO content of the Martian mantle and a low O content in the core (<2-3 wt%), irrespective of magma ocean depth.

References: [1] Rubie D. C. et al. (2004) *Nature, 429*, 58-62. [2] O'Neill H.St.C. et al. (1998) *JGR, 103,* 12239-12260. [3] Ohtani E. and Ringwood A. E. (1984) *EPSL 71*, 85-93. [4] Takafuji N. et al. (2005) *GRL 32*, 6313, doi: 10.1029/2005GL022773. [5] Kesson S. E. et al. (2002) *PEPI 131*, 295-310. [6] Zerr A. et al. (1998) *Science 281*, 243-247. [7] Alfe D. et al. (2002) *EPSL, 195,* 91-98.

NEW SHOCK WAVE DATA PERTAINING TO MAGMA OCEAN THERMODYNAMICS. P.D. Asimow[1] , D. Sun[2], J. Mosenfelder[3], T. J. Ahrens[4] , [1]Caltech 170-25, Pasadena CA 91125, asimow@gps.caltech.edu, [2]Caltech 252-21, Pasadena CA 91125, sdy@gps.caltech.edu, [3]Caltech 170-25, Pasadena, CA 91125, jed@gps.caltech.edu, [4]Caltech 252-21, Pasadena CA 91125, tja@caltech.edu.

New and reinterpreted shock wave data for crystalline SiO_2, Mg_2SiO_4, and $MgSiO_3$ yields melting points of 4700 K at 75 GPa for SiO_2-stishovite and 4900K at 115 GPa for SiO_2 in the $CaCl_2$ structure. For $MgSiO_3$ we infer broad maximum peak in the melting temperature of perovskite structure crystal of 5300 K at 140 GPa. At 170 GPa $MgSiO_3$ enstatite driven into the perovskite structure melts at 5000 K with a 2-3 % increase in density. Mg_2SiO_4 driven into the perovskite plus periclase phase melts at 4150 ± 100 K at 153 GPa.

New data for forsterite and wadlseyite shocked into the melt regime yields a Grüneisen parameter that increased with compression as predicted by [1] such that a silicate melt will yield a ~2000 K adiabatic rise in temperature over the pressure range of a deep magma ocean.

Recent measurements on molten $An_{0.64}Di_{0.36}$, a simplified basalt composition, taken to 110 GPa shows greater compression of the liquid than the solid up to 50% compression range. Thus we find that basaltic liquids are denser than the coexisting ultramafic solids over the entire pressure range existing in the mantle, and effectively extends the Stolper et al. [2] hypothesis to a very wide range of pressures.

References: [1] Stixrude, L. and Karki, B. (2005) Science 310**,** 297-299. [2 Stolper, E. M. *et al.* (1981) J. Geophys. Res. 86**,** 6261-6271.

Percolation of FeS Melts in Partially Molten Peridotite

Bagdassarov N., Golabek G. Institut für Geowissenschaften, Universität Frankfurt Feldbergstrasse 47 60323 Frankfurt a. Main, Germany
Solferino G., Schmidt M. W. Institute for Mineralogy and Petrology, ETH Zürich, Clausiusstrasse 25, 8092 Zürich, Switzerland

The mechanism which provides the segregation of molten Fe-FeS into the core of the Earth is still not fully understood. Due to the high interfacial energy between FeS melts and peridotite material the percolation flow of sulphide melts is not efficient. Two series of percolation experiments have been done on partially molten fertile garnet peridotite, sampled from a xenolith. Powders with 100-200 μm and 20-30μm grain size were mixed with 5-15 vol% Fe-FeS eutectic composition. The deformed high-T garnet peridotite with Mg# 0.90 is composed from 60 vol% Ol, 15% Opx, 5.3 % Cpx and 19% Ga. The first type of experiment has been realized in the centrifuging piston cylinder at ETH, Zürich. The samples of fertile peridotite and $Fe_{70}S_{30}$ powders were sealed in graphite capsules 2.6 mm in diameter and 3 mm in heigh and annealed at 0.8-1 GPa at temperatures of 1150-1260°C in a conventional piston-cylinder over 70 h. Then, the capsules have been rotated in a piston-cylinder at 500 g during 2-10 h at a pressure of 1 GPa and high temperature. Polished sections of samples were analysed on a JEOL microprobe and the distribution of $Fe_{70}S_{30}$ melts and silicate partial melts has been quantified. In the second type of experiments, the powder mixtures of peridotite and $Fe_{70}S_{30}$ were annealed at 1 GPa and at temperatures from 950 to 1300°C in a conventional piston-cylinder and the electrical conductivity of samples has been measured using the impedance spectroscopy method in BN-graphite-CaF_2 pressure cell with concentric cylindrical electrodes made from Mo-foil which corresponds to the oxygen fugacity about IW buffer.

The centrifuge experiments revealed a negligible percolation of $Fe_{70}S_{30}$ melts through the partially molten peridotite matrix. Only at 1260°C and starting 5 vol% of $Fe_{70}S_{30}$ the vertical gradient achieved 1-2 vol%/mm, and in samples with starting 15 vol% FeS the vertical separation achieved 2-2.5 vol%/mm after 10 h of centrifuging. The degree of partial melting of peridotite contributes only in the increase of $Fe_{70}S_{30}$ droplet size, in agreement with the results of Yoshino & Watson (2005). In conductivity experiments, during the 1st heating cycle, the initially high conductivity of powder samples drops for 1-1.5 orders of magnitude within 1h after the reaching of the melting point of $Fe_{70}S_{30}$. Below c. 1000°C the activation energy of electrical conductivity is about that of a peridotite sample, 2.2 eV. Above the melting point of $Fe_{70}S_{30}$ the activation energy slightly increases to 2.35 eV, and then drops to 0.6-0.7 eV above the melting point of peridotite. In contradiction to Yoshino et al. (2004), the electrical conductivity measurements demonstrated that the 5-15 vol% $Fe_{70}S_{30}$ melts never built an interconnected pattern in a peridotite matrix.

EVOLUTION OF THE ENSTATITE CHONDRITE EH4 INDARCH AT HIGH PRESSURE AND TEMPERATURE: NEW EXPERIMENTAL RESULTS

S. Berthet[1,2], V. Malavergne[1,2], K. Righter[3]
[1]Lunar and Planetary Institute, Houston, Texas 77058 et [2]Université de Marne La Vallée, Laboratoire des Géomatériaux, Champs-Sur-Marne, 77454 Cedex, France. E-mail : berthet@lpi.usra.edu. [3]NASA Johnson Space Center, Houston, Texas 77058

Introduction: Chondrite groups are characterized by variations in bulk composition and oxidation state, illustrating in part heterogeneity in the early solar nebula. Planetary accretion and differentiation are two events which, in the planetary sciences, have been debated for at least 25 years and raised many questions. Among diverse models proposed for the accretion of planets, two could be cited: homogeneous accretion [1] and heterogeneous accretion [2,3]. For the particular case of the Earth, the building material of our planet is still not well constrained. Some studies (e.g. [2,3]) assume that one component is highly reduced material, comparable to enstatite chondrites. Thus, for a better understanding of early differentiation processes, it is required to simulate them experimentally. The study of a primitive chemical system under variations of pressure P, temperature T and oxygen fugacity fO_2 remains a good way to identify the phase relations between minerals, their melting products and their interactions with metal. This kind of study allows the understanding of the evolution of a material while the planetary body is growing. Melting relations and equilibrium partitioning behavior have been extensively studied on peridotitic and chondritic starting compositions up to P-T conditions corresponding to the transition zone and lower mantle [4,5,6]. Enstatite chondrites, which are highly reduced primitive meteorites, had never been studied experimentally under such conditions. The first experimental results from the study of the enstatite chondrite EH4 Indarch were introduced by [13]. Since then, further piston-cylinder (PC) (up to 3 GPa and 1700°C) and multi-anvil (MA) (up to 25 GPa and 2500°C) experiments have been performed on the EH4 chondrite Indarch. New experimental results are presented here.

Experimental and analytical methods: The natural starting material Indarch was grounded and doped with a selection of various trace elements (lithophiles, siderophiles, rare earth) in order to extract trace element partitioning data.The PC experiments were carried out at the NASA Johnson Space Center (Houston, USA) and the MA experiments were carried out in two parts: the first one (pressures between 3 and 15 GPa) in a 880-ton press at the NASA Johnson Space Center and the second one (P>20 GPa) in a 1200-ton press at the Bayerisches Geoinstitut (Bayreuth, Germany). All samples were observed and then analysed by scanning electron microscopy equipped with an energy-dispersive X-ray analyzer (EDX) and by electron probe microanalyser (EPMA) equipped with wavelength dispersive X-ray spectrometer (WDX).

Results: Our first PC results indicate that at 1GPa-1500°C and 1GPa-1700°C, the metallic phase is characterized by the presence of two Fe rich liquids (Fig.1(a)): one is S rich, the other one is S poor. At 1500°C, the silicate phase is partially molten whereas at 1700°C, it is all liquid. Between 20 and 25 GPa and up to 2400°C, the silicate material is majoritic garnet or perovskite in equilibrium with a silicate liquid (Fig1(b)) and the Fe-S metallic phase is always liquid, showing some typical quenched melt structures [9]. For these last P-T conditions, the evolution of the partition coefficients (wt% in solid silicate/wt% in liquid silicate) with pressure and temperature has been determined for chromium Cr and manganese Mn between solid silicate (garnet Gt) and silicate liquid (sl). The results for these two elements are presented on Fig.2 and compared to previous studies. EPMA analyses revealed the homogeneity of the metallic and silicate phases of the run products, suggesting that the run durations were sufficient to achieve chemical equilibrium. Despite the effort to maintain the very reducing conditions prevailing during Indarch formation (ΔIW ~ -5.9 [8]), the results show that all the samples have been oxidized during the experiments around ΔIW-2, or ΔIW-3 for the most reduced ones, so that they range between 2 and 3 log units below the iron-wüstite buffer (IW).

Discussion: The results of the present study allow the determination of the preliminary P-T phase diagram of Indarch compared to the ones of the carbonaceous chondrite CV3 Allende and the KLB-1 peridotite (Fig.3). This illustrates the first high pressure and high temperature melting relations of an EH chondrite following the study by [8] of this material at atmospheric pressure. Our first results for Cr and Mn are in good agreement with previous studies (Fig.2). Thus these partition coefficients are not mainly controlled by redox conditions, or the silicate liquid composition. The Gt/sl partition coefficients decrease weakly with increasing pressure (Fig.2(a)). Within the pressure range 20-26 GPa, K_d^{Cr}Gt/sl = 1.39±0.6 and K_d^{Mn}Gt/sl=0.69±0.45. Moreover, the Fig.2(b) does not show evidence of temperature dependence of the Gt/sl

partition coefficients for Cr and Mn. A further study of the elemental (minor or trace) partitioning behavior between the metallic and silicate phases over the pressure range 0-25 GPa and the temperature range between subsolidus and superliquidus conditions should allow to derive new constraints on the understanding of early planetary differentiation processes.

References: [1] Ringwood A.E. (1979) *Origin of the Earth and Moon*. [2] Wänke H. and Dreibus G. (1988) *Phil. Trans. R. Soc. Lond., A325*, 545-557. [3] Javoy M. (1995) *GRL, 22*, 2219-2222. [4] Takahashi E. (1986) *JGR, 91*, 9367-9382. [5] Agee C.B. et al. (1995) *JGR, 100*, 17725-17740. [6] McFarlane et al. (1994) *GCA, 67*, 5161-5172. [7] Lee J. and Morita K. (2002) *ISIJ International, 42*, 588-594. . [8] McCoy T. et al. (1999) *Meteoritics & Planet. Sci., 34*, 735-746. [9] Siebert J.et al. (2004) *PEPI.,144*, 421-432. [10] Zhang J. and Herzberg C. (1994) *JGR, 99*, 17729-17742. [11] Asahara Y. et al. (2004) *PEPI, 143-144*, 421-432. [12] Tronnes R. and Frost D. (2002) *EPSL 197*, 117-131. [13] Berthet S. et al.. (2006) *LPSC XXXVII*, Abstract #2026.

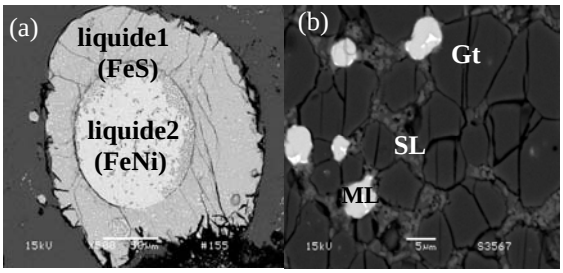

Fig.1 : Back-scattered electron images: (a) a PC run product (1 GPa, 1500°C, 2 hours), the metallic phase is composed of two liquids: a Fe-Ni alloy core and a Fe-S ring. (b) a MA run product (20 GPa, 2000°C, 5 min), two silicate phases are present: majorite crystals (Gt) and a silicate liquid (sl).

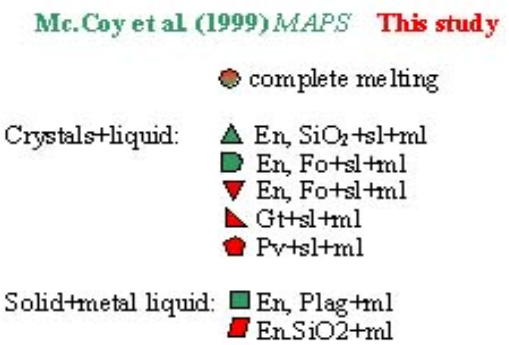

Legend of Fig.3

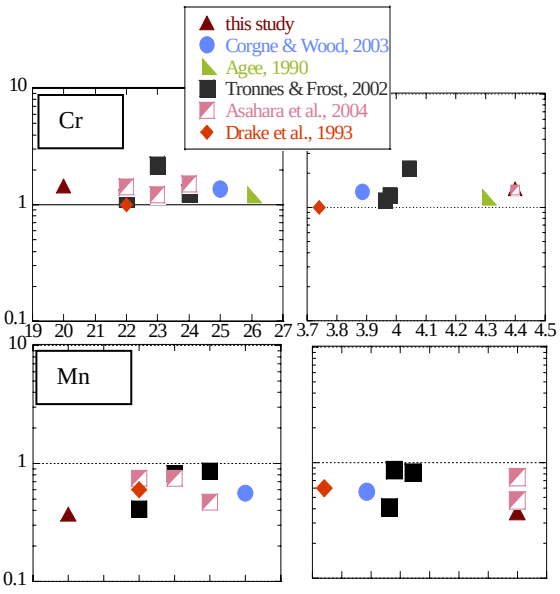

(a) $K_d^{Gt/sl}$ vs P (GPa) (b) $K_d^{Gt/sl}$ vs 10^4/T (K^{-1})

Fig. 2: Experimental results of this study and previous work for Cr and Mn. (a) The K_d^{Cr} et K_d^{Mn} between Gt et sl are plotted vs P. (b) The K_d^{Cr} et K_d^{Mn} between Gt et sl are plotted vs T.

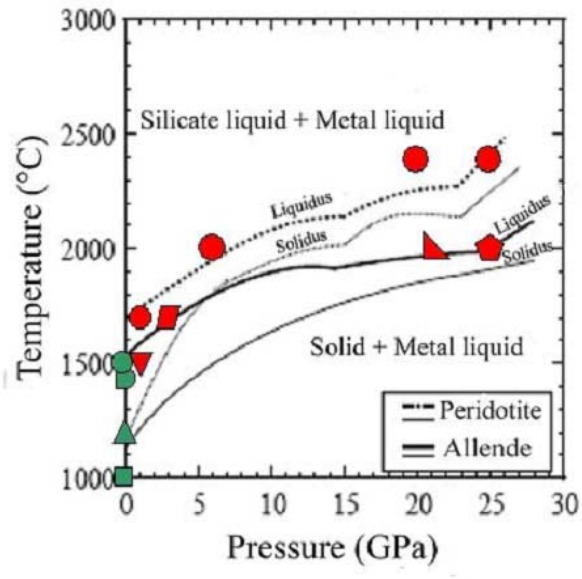

Fig. 3 : P-T phase diagram of Indarch compared to the ones of the Allende meteorite and the KLB-1 peridotite. Liquidus and solidus of Allende between 0 and 20 GPa are given by [5] and those above 20 GPa by [11]. Liquidus and solidus of the peridotite between 5 and 20 GPa are given by [10] and those above 20 GPa by [12].

THE DIFFERENTIATION HISTORY OF MARS INFERRED FROM ISOTOPIC STUDIES OF SNC METEORITES. Lars. E., Borg [1]Lawrence Livermore National Laboratory, 7000 East Avenue, Livermore CA 94550 (lborg5@llnl.gov).

Introduction: The differentiation history of a planet is primarily concerned with the timing and mechanisms by which planetary reservoirs, such as core, mantle, and crust, are formed. This history is a prelude to how these reservoirs interact and how lithological, geochemical, and isotopic diversity is produced in the rock record of an individual body. The differentiation history of the terrestrial planets is most clearly inferred from rock samples. In the case of Mars, these are the S (Shergotty), N (Nakhla), and C (Chassigny) meteorite suite. Although the shergottites (hereafter referred to martian basalts) have a very limited range of ages, defining only 3 age categories (174 ± 2 Ma; N = 11; 333 ± 9 Ma, N=4; 474-575 Ma N = 3; [1]) they display large compositional and isotopic variations. As a consequence they are ideal to constrain processes of martian planetary differentiation and evolution. The goal of this abstract is use the petrological, geochemical, and isotopic characteristics of the martian basaltic meteorite suite to: (1) outline the differentiation history of Mars and (2) present a petrogenetic model for the origin of these basalts. This represents a synthesis of ideas presented by our group over the last 10 years.

Critical Observations that Constrain Differentiation: There are four main observations that constrain the differentiation of Mars. First, martian basalts demonstrate a huge range of compositional and isotopic variability [Fig. 1]. Furthermore, the basalts fall into three subgroups distinguished by their geochemical characteristics which indicate derivation from incompatible-element depleted, incompatible-element enriched, and intermediate source regions. These large elemental fractionations suggest that the fractionation processes that produced the source regions of these basalts were very efficient. It further suggests that homogenization of the source regions by recent geologic processes has been minimal or has not occurred.

The second observation is that the element and isotopic systematics of the source regions of the martian basalts appear to define binary mixtures between incompatible-element-depleted mantle-like reservoirs and evolved incompatible-element-enriched reservoirs [Fig. 2]. Geochemical and isotopic similarities between the source regions of the martian basalts and lunar samples again suggest that martian and lunar sources were produced by similar processes.

Third, the source regions of these basalts formed very early in the history of the solar system. A model age of differentiation of $4526\ ^{+21}_{-19}$ Ma [1] is defined on the ε^{142}_{Nd} - ε^{143}_{Nd} diagram below [Fig. 3]. Such rapid and extensive differentiation of basaltic sources is suggests formation via magma ocean solidification [2, 3, 4].

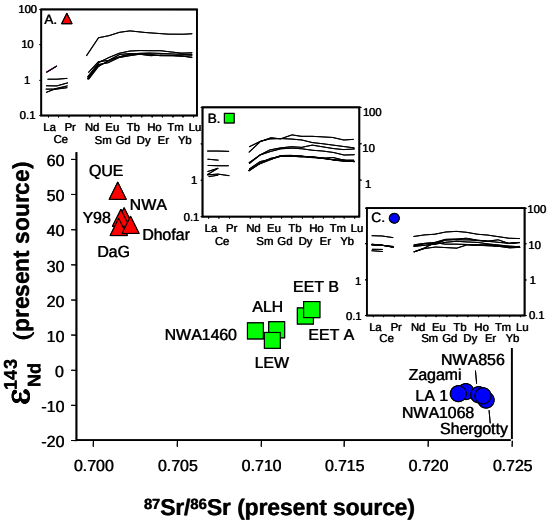

Figure 1. Present-day $^{87}Sr/^{86}Sr$- ε^{143}_{Nd} plot of shergottites illustrating three distinct suites of samples. Filled triangles are oldest shergottites with strongly LREE-depleted REE patterns and inset A depicts their REE patterns. Green squares are shergottites with intermediate REE and Sr-Nd isotopic systematics and inset B depicts their REE patterns. Filled circles are ~175 Ma shergottites with the most LREE enriched patterns and sources with the most radiogenic Sr and least radiogenic Nd isotopic compositions. Inset C depicts their REE patterns. Data summarized in [1].

The fourth and final observation is that the trace element and isotopic systematics of the martian basalts do not correlate, suggesting that the Sr and Nd isotopic compositions and REE patterns observed in the martian basalts are not controlled by assimilation-fractional crystallization process occurring in the martian crust [6]. It is therefore probable that the mixing processes observed in the martian meteorite suite are not accompanied by large extents of fractional crystallization and that these mixing relations reflect processes occurring in the martian mantle.

Production of Martian Basalt Source Regions: Geochemical modeling completed by [2, 3, 4] indicates that the source regions of the martian basalts can be produced by solidification of a magma ocean. These models calculate the major and trace element composition of cumulates formed from solidification of a roughly chondritic composition. Early solidification

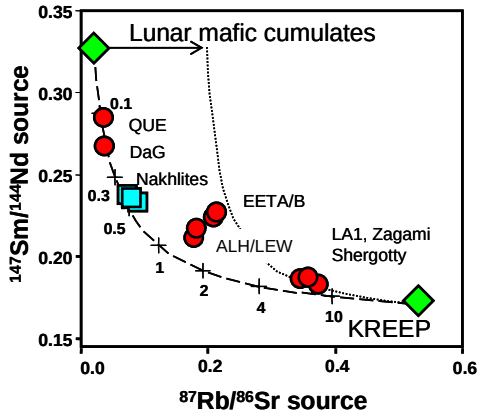

Figure 2. Binary mixing diagram of the source regions of individual martian basalts calculated from their initial Sr-Nd systematics after [a]. Lunar source compositions from [5].

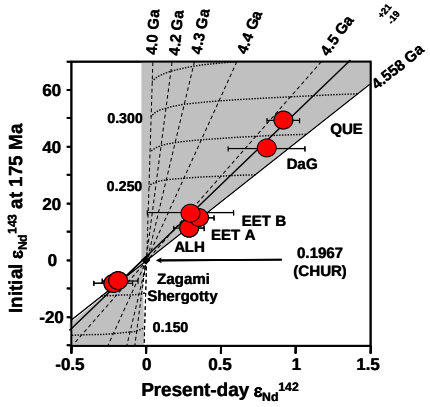

Figure 3. Two-stage Nd isotope evolution model indicating that martian differentiation occurred at 4526 Ma. Reproduced from [2].

and removal of majoritic garnet leaves the remaining liquid depleted in Al. Subsequent solidification of this liquid produces cumulates with a range of compositions and mineralogies. Partial melting of these cumulates reproduces the major element abundances of the most primitive martian parental melts, and the trace element and isotopic systematics of the most LREE-depleted martian basalts. Late-stage crystallization products of this modeled magma ocean are enriched in incompatible elements and have characteristics that are very similar to lunar KREEP. Mixing between the early and late stage magma ocean crystallization products reproduces the mixing arrays observed in the martian basalt suite. The ability of these models to reproduce the major element and isotopic systematics of the basalt suite, combined with evidence for rapid and efficient differentiation of the basalt source suggests that differentiation of Mars occurred via solidification of a magma ocean.

Major Element Variability of Martian Basalts: The major element compositions of the individual meteorites demonstrate a wide range of Mg#'s that do not correlate with the REE systematics or the initial Sr-Nd isotopic systematics of the martian basalts [Figure 4].

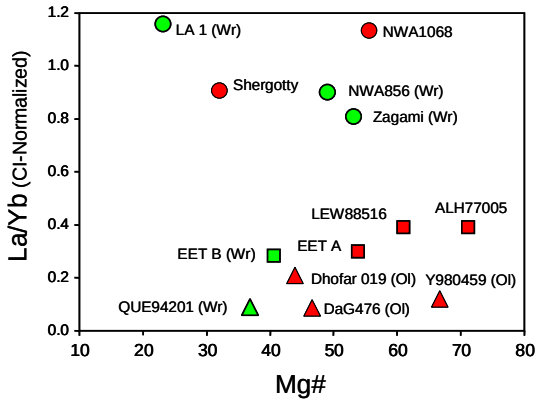

Figure 4. Whole-rock values of chondrite normalized La/Yb ratios vs. Mg# (=$[MgO/(MgO+FeO)]_{molar}$) of shergottite whole rocks or calculated for shergottite parental liquids. Symbols correspond to subgroup classification: triangles are samples that have isotopic and rare-earth element systematics indicative of derivation from incompatible-element-depleted source regions, circles are derived from incompatible-element-enriched source regions, and squares are derived from source regions with intermediate incompatible-element systematics (see text).

This lack of correlation suggests that the difference in major element compositions of the meteorites does not reflect compositional variability in the source regions. Instead, it suggests that major element abundances are controlled by fractional crystallization of the parental magmas once they leave their source regions. This is supported by the observation that major element modeling using the MELTS algorithm and trace element modeling using simple fractional crystallization models are able to reproduce the compositions of martian basalts belonging to individual subgroups. This has been most clearly illustrated for the incompatible element-depleted subgroup by [6]. They noted that ~40% crystallization of a parental magma with a composition of Y980459 reproduces the composition of QUE94201.

Summary: Martian basaltic source regions formed early in the history of the planet as a result of crystallization of a magma ocean. Mixing between these sources is responsible for broad differences in their incompatible element and isotopic systematics. The major element compositions of the basalts are controlled by the extent of fractional crystallization parental magmas underwent after leaving the mantle.

References: [1] Borg & Drake, (2005) *JGR* **110,**.E12SO3; [2] Borg et al. (1997) *GCA* **61,** 4915; [3] Borg et al. (2003) *GCA* **67,** 3519; [4] Borg & Draper (2005) *MAPS* **38,** 1713; [5] Snyder et al., (1992) *GCA* **56,** 3809; [6] Symes et al. (2005) LPSC **36,** Abstr. #1435.

EARLY PLANETARY DIFFERENTIATION: UNMIXING AND REMIXING PLANETARY INTERIORS.

Richard W. Carlson[1] and Maud Boyet[1,2], [1]Carnegie Institution of Washington, Department of Terrestrial Magnetism, 5241 Broad Branch Road, NW, Washington, DC, 20015, USA, carlson@dtm.ciw.edu, [2]Transferts Lithospheriques, UFR Sciences et Techniques, 23 Rue du Docteur Paul Michelon, 42023, Saint Etienne, France.

Introduction: Evidence that massive chemical differentiation of a planet could occur became available in the 1800's with the recognition that the Earth has a dense metal core and an overlying silicate mantle [1]. That core-mantle differentiation occurred early in Earth history was shown by Patterson's first "age of the Earth" calculations [2]. Defining how early the segregation of metal from silicate took place has become possible only in the last decade through the advent of Hf-W studies that show that asteroidal cores formed within 1-3 Myr of solar system formation [3] and that the cores of large planets, such as Earth, took only a few tens of millions of years to form [4].

That these early chemical differentiation events extended into the silicate portions of planet(esimal)s did not become obvious until the study of the returned lunar samples. On the Moon, the chemical complimentarity between aluminous crust and the mantle source of mare basalts led to the concept of a lunar magma ocean [5] that radiometric data show to have completed its differentiation by ~4.4 Ga [6,7]. Recent work with a variety of short-lived radiometric chronometers shows clearly that Mars, the Moon, and the HED parent body segregated chemically distinct crusts and mantles within 1 to 25 Myr of the birth of the solar system [e.g. 4]. The very short time scale over which early planetary differentiation occurred lessens one of the major objections to this process – the energy source needed to melt a growing planet. Since planetary differentiation appears to have begun within 1-2 Myr of solar system formation, extinct radioactivity (e.g. 26Al and 60Fe), the kinetic energy of accumulation, and the gravitational potential energy of rapid core segregation all could serve as sufficient energy sources for global differentiation.

Surprisingly, evidence for early differentiation of the silicate Earth is remarkably muted. Most recent discussions of magma ocean consequences on the Earth focus more on core-mantle equilibrium than on internal differentiation of the silicate portion of our planet [e.g. 8]. The persistence of the idea that much of Earth's mantle still contains chondritic relative abundances of refractory lithophile elements, with only a portion of the mantle depleted by the growth of continental crust over Earth history [e.g. 9], is testimony to the ambiguity of geochemical indicators for early differentiation of the silicate Earth. Does this mean that the silicate Earth did not experience an early differentiation event or does it instead indicate that the consequences of this event have been blurred either because crystal-liquid separation is inefficient in a large, actively convecting, planet [10] or because convection in Earth's interior efficiently mixed away the chemically distinct reservoirs formed in an early differentiation?

Evidence for Early Terrestrial Differentiation: Improvements in isotope ratio precision have recently allowed clear delineation of variations in 142Nd/144Nd in some Eoarchean rocks [11,12] caused by the decay of 103 Myr half-life 146Sm. In addition, all terrestrial rocks so far measured have higher 142Nd/144Nd than chondrites [13]. Three explanations may explain the offset of the terrestrial and chondritic Nd data:

1) The 142Nd deficit in chondrites is not related to 146Sm decay, but reflects nucleogenic isotope anomalies in poorly mixed solar system materials [14]. Our new measurements of carbonaceous chondrites confirm deficits in 142Nd/144Nd of up to 40 ppm compared to terrestrial Nd that cannot be accounted for by variations in Sm/Nd. However, several ordinary chondrites that have 142Nd/144Nd 18 ± 1 ppm lower than terrestrial, have Sm isotopic compositions indistinguishable from terrestrial [15, 16]. This supports the idea that the high 142Nd/144Nd of Earth compared to O-chondrites is the result of 146Sm decay in a high Sm/Nd (i.e. incompatible element depleted) reservoir.

2) The Earth has a Sm/Nd ratio (147Sm/144Nd = 0.209) about 6% higher than the average measured for chondrites. Chondrites display a very narrow range in Sm/Nd (approximately +/- 3% about the mean), and no whole chondrite measurement yet reported has Sm/Nd as high as needed to explain the 142Nd/144Nd measured for most terrestrial rocks. An Earth with Sm/Nd 6% higher than average chondrite would have present day 143Nd/144Nd = 0.51301, which is only slightly lower than measured for MORB and is equal to the most common value found for ocean island basalts. This result would suggest that the major volume of the Earth's mantle is depleted in incompatible elements, and that no material similar to previous estimates of bulk-silicate earth (BSE) composition [17] remain.

3) If the BSE does, in fact, retain chondritic relative abundances of refractory lithophile elements, then the superchondritic 142Nd/144Nd of all terrestrial rocks measured so far would require that the portion of Earth's mantle that supplies crustal rocks had its

Sm/Nd ratio increased while 146Sm was still alive – our estimates place this event at prior to 4.53 Ga [13]. This would then also require the existence of a reservoir within the Earth with 142Nd/144Nd less than chondritic. We have been searching for evidence of such a reservoir, and have measured suggestively low 142Nd/144Nd in kimberlites that plot to the low 176Hf/177Hf side of the Nd-Hf mantle array [18], but the data are not yet clearly resolved from the "normal" terrestrial value.

Lunar Evidence for Early Terrestrial Differentiation: In contrast to a recent study of 146Sm-142Nd systematics of lunar rocks [19], but in support of a previous study [20], we find that the 142Nd/144Nd data for lunar rocks suggests that the early evolution of the Moon was characterized by an even higher Sm/Nd than postulated for the Earth's early depleted reservoir. This is shown most clearly in the data for two crustal rocks, the ferroan anorthosite 60025, and high-Mg suite norite 78236, where a 2-point line fit to whole rock Sm-142Nd measurements for these samples gives an age of 4459 Ma, within error of their 147Sm-143Nd isochron ages [21,22], but with an initial 142Nd/144Nd 34 ppm higher than average O-chondrite. This would require a 147Sm/144Nd of between 0.23 and 0.24 for the early Moon, which, though some 20% higher than chondritic, is within the range previously predicted on the basis of the high initial 143Nd/144Nd of lunar crustal rocks [23]. In contrast, KREEP and mare basalt data define a slope on a 142Nd/144Nd diagram consistent with an "age" of over 200 Myr after solar system formation suggesting that the magma ocean persisted long after the lunar crust formed. In our data, this isochron gives an initial 142Nd/144Nd only 23 ppm higher than average O-chondrite, implying that the Sm/Nd ratio of the lunar interior decreased between the 4.44 Ga age of crust formation and the ~4.35 Ga age indicated by the KREEP – mare basalt isochron.

Remixing the Products of Early Differentiation: Our lunar 142Nd/144Nd thus suggest that an initially highly depleted lunar interior became less depleted with time. A similar progression is observed in Eoarchean rocks from Isua, Greenland that have 142Nd/144Nd 15 ppm higher than found in all post-Eoarchean rocks [11,12]. The most straightforward explanation of this observation is that an early differentiation event on both the Earth and Moon initially created highly incompatible-element-depleted (high Sm/Nd) and complementary incompatible-element-enriched (low Sm/Nd) reservoirs, and that some portion of the enriched material was mixed back into the depleted reservoir. In the Earth, the persistence of the early formed heterogeneity is recorded in rocks as young as 3.8 Ga. The long duration required for this "remixing" of the Earth's mantle suggests that the process causing the mixing of early-formed depleted and enriched reservoirs was solid-state convection.

Fate of the Enriched Reservoir: If the BSE has chondritic relative abundances of refractory lithophile element abundances, then the 18 ppm excess 142Nd/144Nd of most terrestrial rocks compared to O-chondrites shows that this remixing has been incomplete and that an incompatible-element-rich reservoir still exists within Earth's interior. A more speculative alternative is that an incompatible-element-rich primordial crust on Earth could have been largely removed from the Earth-Moon system by the giant impact that formed the Moon largly out of the early-formed depleted terrestrial mantle.

References: [1] Brush S.G. (1980) *Am. J. Phys.,* 48, 705-724. [2] Patterson C.C. (1956) *Geochim. Cosmochim. Acta*, 10, 230-237. [3] Markowski A. et al. (2006) *Earth Planet. Sci. Lett.,* 242, 1-15. [4] Halliday A.N. and Kleine T. (2006) *MESS-II*, Lauretta D.S. and McSween, H.Y., eds., 775-801. [5] Taylor S.R. and Jakes P. (1974) *Proc. 5th Lunar Sci. Conf.*, 1287-1305. [6] Tera F. and Wasserburg G.J. (1974) *Proc. 5th Lunar Sci. Conf.,* 1571-1599. [7] Carlson R.W. and Lugmair G.W. (1981) *Earth Planet. Sci. Lett.*, 52, 227-238. [8] Righter K. and Drake M.J. (2003) in, *Treatise of Geochemistry*, 425-445. [9] Wasserburg, G.J. and DePaolo D.J. (1979) *Proc. Nat. Acad. Sci.*, 76, 3594-3598. [10] Solomotov V.S. (2000) in, *Origin of the Earth and Moon*, R.M. Canup and K. Righter, eds., 323-338. [11] Caro G. et al. (2003) *Nature*, 423, 428-432. [12] Boyet M. et al. (2003) *Earth Planet. Sci. Lett.*, 214, 427-442. [13] Boyet M. and Carlson R.W. (2005) *Science,* 309, 576-581. [14] Ranen M.C. and Jacobsen S.B. (2006) *Lunar Planet. Sci.* XXXVII, 1832. [15] Andreasen R. and Sharma M. (2006) *Science*, in press. [16] Boyet M. and Carlson R.W. (2006) *Earth Planet. Sci. Lett.,* in press. [17] McDonough W.F. and Sun S.-S. (1995) *Chem. Geol.*, 120, 223-253. [18] Nowell G.M. et al. (2004) *J. Pet.*, 45, 1583-1612. [19] Rankenburg K. et al. (2006) *Science*, 312, 1369-1372. [20] Nyquist L.E. et al. (1995) *Geochim. Cosmochim. Acta*, 59, 2817-2837. [21] Carlson R.W. and Lugmair G.W. (1988) *Earth Planet. Sci. Lett.*, 90, 119-130. [22] Nyquist L.E. et al. (1981) *Proc. Lunar Planet. Sci.,* 12B, 67-97. [23] Borg L. et al. (1999) *Geochim. Cosmochim. Acta,* 63, 2679-2691.

EXPERIMENTAL CONSTRAINTS ON PLANETARY CORE FORMATION IN AN EARLY MAGMA OCEAN. Nancy L. Chabot[1], [1]JHU Applied Physics Laboratory, 11100 Johns Hopkins Road, Laurel, MD, 20723-6099, nancy.chabot@jhuapl.edu.

Introduction:

It has been proposed that the early differentiation of Earth involved core formation in a magma ocean, where molten metal separated from liquid silicate, such as depicted in Fig. 1. Interpreting the abundances of siderophile, metal-loving, trace elements in Earth's mantle can provide insight into the core formation process. Experiments examining the partitioning behaviors of these trace siderophile elements between liquid metal and liquid silicate not only test the theory of core formation in a magma ocean but also have the potential to constrain the conditions present in an early magma ocean on Earth.

Numerous studies (reviewed by [1]) have provided information about the metal/silicate partitioning behavior of siderophile elements; the results have shown that pressure, temperature, oxygen fugacity, and metal and silicate compositions can all have a significant influence on an element's metal/silicate partition coefficient (D). Additionally, different elements are affected differently by these thermodynamic variables. Thus, by combining the constraints from multiple elements, unique information about the core formation process can be obtained.

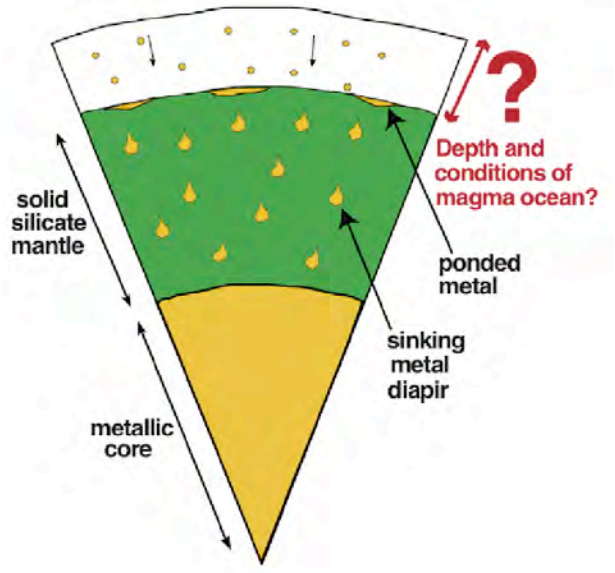

Figure 1. *This illustration depicts core formation in an early magma ocean. Fundamental information about the conditions of this scenario, such as the depth, temperature, oxygen fugacity, and compositions involved, can be constrained with metal/silicate partitioning experiments.*

Experimental Approach:

Figure 2 shows a typical experimental run product; liquid metal and liquid silicate are brought to the desired conditions and allowed to equilibrate. The experiments are then quenched and the compositions of the bulk metal and bulk silicate are measured to determine an element's metal/silicate partition coefficient. Systematic sets of experiments can be conducted to isolate the effects of pressure, temperature, oxygen fugacity, and composition.

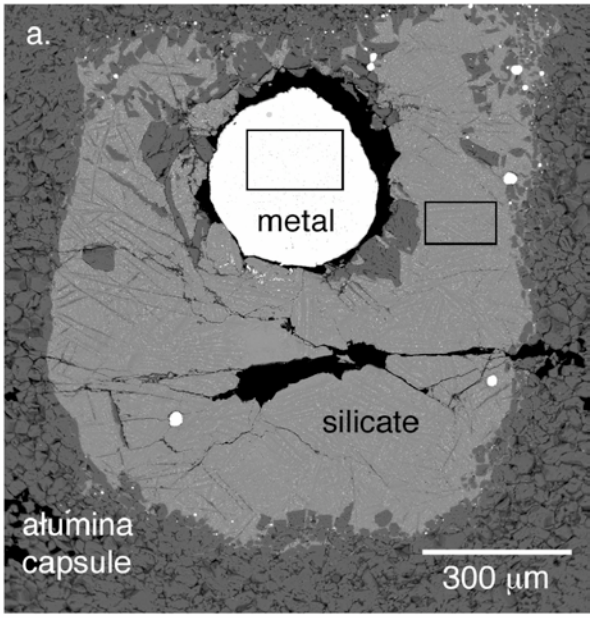

Figure 2. *A back-scattered electron image of this run product illustrates the typical experimental approach to metal/silicate partitioning experiments. Experiments contain well-separated metal and silicate phases, both liquids at run conditions, as encountered during core formation in a magma ocean. Figure taken from [2].*

Constraints from Ni and Co:

The elements of Ni and Co have been the focus of many previous studies (reviewed in [2]) and are a good starting point because of some simplifications they offer. For one, the metal/silicate partitioning behaviors of Ni and Co have been found to be largely independent of both the silicate composition and the metallic composition for light element concentrations appropriate to Earth's core. Additionally, Ni and Co have been demonstrated to behave as divalent elements over the range of oxygen fugacities relevant to Earth's core formation. Using experiments to determine the effects of pressure and temperature, D(Ni) and D(Co) can be

parameterized as a function of oxygen fugacity, pressure, and temperature and used to explore possible core formation conditions. Figure 3 shows the large range of pressure and temperature combinations where the mantle abundances of Ni and Co are consistent with being set by liquid metal, liquid silicate equilibrium. The results from Ni and Co thus lend support to the magma ocean core formation scenario but provide limited constraints on the conditions present at that time.

Constraints from other elements:

V, Cr, and Mn. The elements of V, Cr, and Mn show minor depletions in Earth's mantle relative to chondritic abundances. Experimentally based parameterizations of D(V), D(Cr), and D(Mn) suggest that these depletions can be matched at high, 2500-4000 K, temperatures and the partitioning of all three elements are relatively pressure independent [3, 4]. However, because these elements exhibit only minor depletions in Earth's mantle, the specific depletions are more affected by the choice of bulk Earth chondritic composition. Additionally, the higher volatility of Mn, and to a lesser extent Cr, further complicates estimating the depletions due to core formation. Thus, understanding the mantle abundances of V, Cr, and Mn offer insight into the evolution of Earth but do not provide as tight constraints on core formation as the truly siderophile elements.

Sulfur. Similar experimental studies have reached opposite conclusions about whether the S concentration in Earth's mantle is consistent with being set by core formation in a magma ocean [5, 6]. However, previous experimental studies focused on systems involving S saturation, which is important for basaltic processes but involves much higher S contents than envisioned during Earth's core formation. By accounting for the lower S content during Earth's core formation, it appears that Earth's mantle S abundance is consistent with metal/silicate equilibrium in a magma ocean. Furthermore, conditions between 35-60 GPa and 2500-4000 K appear to be able to explain the mantle abundances of not just S but also Ni and Co. Thus, S has the potential to provide an important constraint on the conditions present during core formation. Currently though, the S partitioning data are limited, especially at low S contents, requiring large extrapolations to be applied to core formation conditions.

W and Mo. As refractory moderately siderophile elements, W and Mo are prime candidates to provide constraints to Earth's core formation. Parameterizations by [7] concluded that the mantle depletions of both elements are compatible with being set by core formation. However, the work of [7] was largely based on 1 atm data, which has been shown to provide unreliable parameterizations to higher pressures and temperatures [2].

Highly Siderophile Elements. The abundances of highly siderophile elements in Earth's mantle are many orders of magnitude higher than predicted by 1 atm partitioning studies. Experiments also frequently create "nuggets" rich in highly siderophile elements. The interpretation of the formation of these nuggets is central to knowing how to apply the results to Earth's core formation and is an area of active research [e.g. 8].

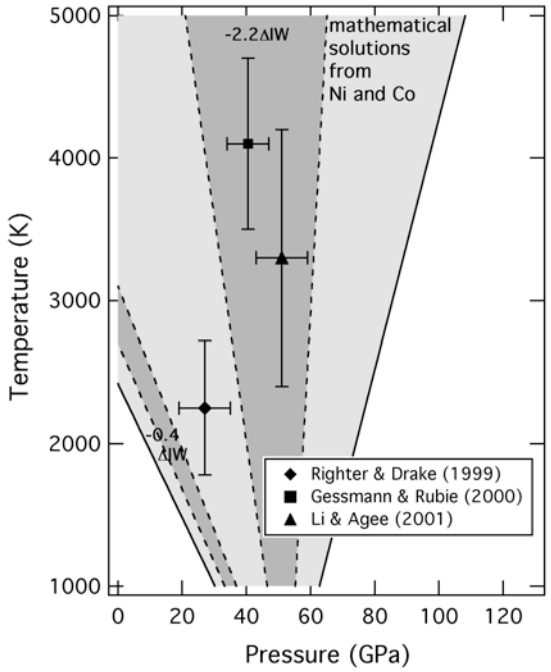

Figure 3. *Constraints on the conditions of core formation in a magma ocean from Ni and Co metal/silicate partitioning are shown. The Ni and Co results suggest that the mantle abundances of these elements are consistent with being set by core formation in a high-pressure magma ocean. However, constraints from additional elements are needed to narrow down the allowable conditions. Figure taken from [2].*

References: [1] Walter M. J. et al. (2000) In *Origin of the Earth and Moon* (R. M. Canup and K. Righter, Eds.), U. of Arizona Press, Tucson, AZ, USA. [2] Chabot N. L. (2005) *GCA* **69**, 2141-2151. [3] Gessman C. K. and Rubie D. C. (2000) *EPSL***184**, 95-107. [4] Chabot N. L. and Agee C. B. (2003) *GCA* **67**, 2077-2091. [5] Li J. and Agee C. B. (2001) *GRL* **28**, 81-84. [6] Holzheid A. and Grove T. L. (2002) *Am. Min.* **87**, 227-237. [7] Righter K. et al. (1997) *PEPI* **100**, 115-134. [8] Cottrell E. and Walker D. (2006) *GCA* **70**, 1565-1580.

Acknowledgements: Supported by NASA grant NNG06GI13G.

PHASE EQUILIBRIA AND MELTING OF PLANETARY ANALOGS: FIRST RESULTS FROM IN SITU HIGH P-T MELTING EXPERIMENTS. L. R. Danielson[1], K. Righter[1], Y. Wang[2], and K. Leinenweber[3]. [1]NASA JSC, Mail Code KT, 2101 NASA Road One, Houston, TX 79058, lisa.r.danielson@nasa.gov, kevin.righter-1@nasa.gov. [2]GSECARS, APS ANL, 9700 South Cass Ave., Bldg. 434A, Argonne, IL 60439, wang@cars.uchicago.edu. [3]Dept. of Chemistry and Biochemistry, Arizona State University, Tempe, AZ 85287-1604, kurtl@asu.edu.

Introduction: Chondritic material is thought to be the fundamental building blocks of terrestrial planets and planetesimals. Therefore, crystallization of chondritic and peridotitic material can be used to simulate accretion and segregation of a bulk planet. Crystallizing phases in a liquid magma ocean, whether persistent or intermittent, could significantly change the composition (and oxidation state) of that liquid by crystal flotation or settling. Also, crystals settling to the core-mantle boundary could provide a source for light elements in the core, or constraints on the abundance of some light elements.

Although chondritic and peridotitic phase equilibria below 20 GPa have been studied in detail [1,2,3,4,5,6], experiments above 20 GPa which constrain the liquidus are lacking. Because this pressure range represents the transition into the Earth's lower mantle, experiments in this pressure range are critical to understanding early crystallization of the deepest planetary mantles. For example, Allende (CV3 carbonaceous chondrite), Richardton (H5 chondrite), and peridotite uncertainty in the liquidus is ~ 200 °C above 20 GPa. There is also disagreement as to the identity of the liquidus phase above 20 GPa, whether it's magnesiowüstite [2] or Mg-Fe perovskite [5], and at what P-T the liquidus phase changes from magnesiowüstite to Mg-Fe perovskite.

In previous phase equilibria experiments, run products represent either a single P-T of interest, or, at P, the modeled capsule thermal gradient is used to determine equilibrium phases at a range of temperatures. In both cases, conditions within the capsule at P-T must be interpreted from quenched run products. Active processes such as convection and melt migration, sluggish melting kinetics, crystal growth, and diffusion on quench can obscure the original phase assemblage in the capsule.

The objective of this study is to measure the liquidus phases and temperatures for a number of planetary mantle analog materials at P > 20 GPa

Experimental: The Advanced Photon Source at Argonne National Laboratory provides the unique opportunity for in situ observation of phase transitions and state change in a single experiment during increasing T, greatly reducing uncertainties of previous experiments. The split-cylinder high pressure module in the 1000 ton Large Volume Press was used to conduct experiments targeted above 20 GPa, and T > 2000 °C.

A 3mm TEL modified Fei-type assembly used in experiments has been developed by Leinenweber and Soignard at Arizona State University for beamline use (Figure 1). This assembly is a Re furnace with lanthanum chromite insulating sleeve, alumina end caps and graphite capsule. Starting materials are a fine powder, packed into the capsule. X-ray windows are a slit in the Re furnace and alumina plugs in the lanthanum chromite. A pressed pellet of MgO powder doped with diamond powder was used as a pressure standard and packed between the capsule and thermocouple.

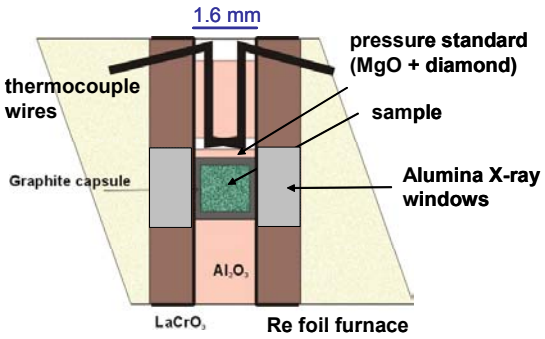

Figure 1. Modified 8/3 assembly for beamline use.

The first set of experiments were conducted on the Allende meteorite, because of its lower melting temperature and conflicting set of previous work. The same run conditions and procedures will in future be applied to experiments using Richardton and peridotite as starting material.

The time at temperatures above 1500 °C and above 400 tons was ~ 55 minutes, and 14 minutes above 2000 °C. The radiography image (Figure 2) shows the end result of compression to 400 tons and heating to a peak temperature of 2200 °C.

Two runs have been successfully completed, one at 400 tons and one at 600 tons. The sample at target tonnage was heated and phases present were identified during increasing T until the sample completely melted. Data were collected every 100 °C from 1500 to 1800 °C and every 50 °C from 1800 to 2200 °C. The sample was quenched from T by turning off the power.

Temperature at the hotspot, the region of interest for analyses, was calculated using the thermal modeling program developed by [8].

Analytical: Phases were identified using energy-dispersive X-ray diffraction (EDXRD). The fixed diffraction angle (2θ) was ~6°. Data collection times at each P and T of interest was 60 seconds. Peak positions were determined by Gaussian fitting after background subtraction. Lattice parameters were obtained from linear regressions to d-spacings.

Results: Pressure determination for the MgO pressure standard was made using two approaches, the Birch-Murnahan equation of state with bulk modulus data of [9] and by using the molecular dynamics simulation of [10]. Pressures were in agreement within 0.5 GPa. Reported pressures here are calculated from [10], after similar work conducted by [11]. Figure 3 shows phases identified by EDXRD.

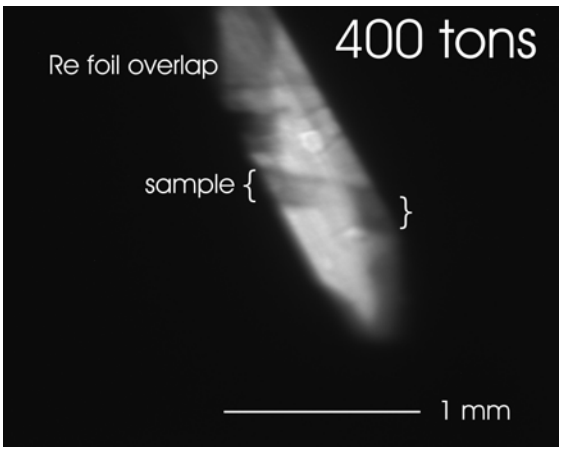

Figure 2. Radiography image of compressed sample though the Re slits and alumina windows. Maximum pressure achieved was 19.1 GPa. The sample is the dark band indicated by curly brackets. The pressure standard was located immediately above the sample. The dark area in the upper left is an area where the slit in the Re foil ends.

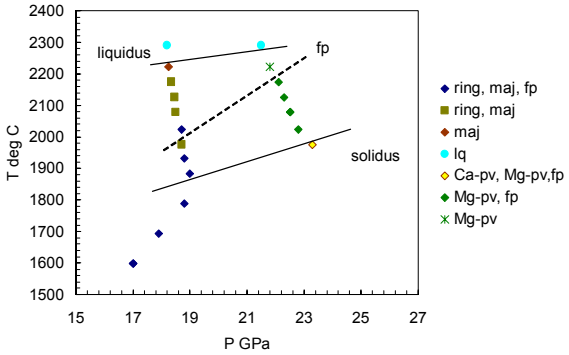

Figure 3. Phase abbreviations are: ring – ringwoodite, maj – majorite garnet, fp – ferropericlase, lq – silicate liquid, Ca-pv – Ca-perovskite, Mg-pv – Mg-perovskite. Lines indicate phase boundaries.

Discussion and Conclusions: The field of melting is larger for the in situ experiments (Figure 4). The majorite liquidus temperature occurs near 2250 °C, compared to previous results of 2000 °C. The majorite-Mg-perovskite cotectic occurs before 22 GPa, as opposed to around 25 GPa. However, given the limited number of experiments and uncertainties introduced from previously not applying (1) a P-T relationship from relaxation of the assembly during heating, and (2) a thermal gradient from temperatures measured at the thermocouple across the capsule, significant differences in P and T are not surprising. It is possible to identify a majorite-ferropericlase cotectic for previous studies at around 22 GPa. This is particularly true for [2], where calibrations were performed at 1200 °C. Pressure at 2000 °C can be 3 GPa lower than that at 1200 °C [12].

Although Mg-perovskite was identified as the liquidus phase above 22 GPa, the ferropericlase-out line is very steep, and may become the liquidus phase above 23 GPa. This is comparable to the results from [13], where the majorite-ferropericlase cotectic occurs at around 2300 °C and 23 GPa.

The higher liquidus temperature with the large liquidus field, would tend to support a shallow magma ocean model with a large zone of crystal mush.

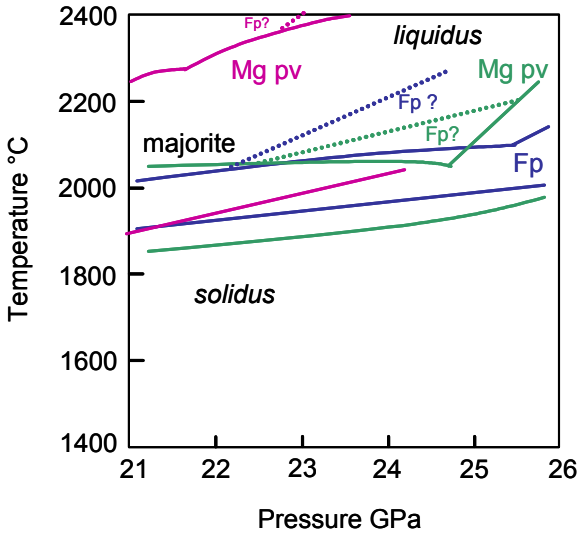

Figure 4. Comparison of Allende phase diagrams, magenta-this study, green-[5], blue-[2]. Dashed lines indicate possible interpretations of the location of a ferropericlase liquidus for each study, given the uncertainties in the experiments.

References: [1]Zhang and Herzberg (1994) *J. Geophys. Res*, 99, 17729-17742. [2]Agee et al. (1995) *J. Geophys. Res.*, 100, 17725-17740. [3]Kavner and Jeanloz (1998) *Geo. Res. Lett.*, 25, 4161-4164. [4]Litasov and Ohtani (2002) *Phys. Earth Planet. Int*, 134, 105-127. [5]Asahara et al. (2004) *Phys. Earth Planet. Int.*, 143-144, 421-432. [6]Danielson et al. (2004) *Eos Trans. AGU*, 85(47), Fall Meet. Suppl., V43C-1432. [7]Lee et al. (2004) *Earth Planet. Sci. Lett*, 223, 381-393. [8]Hernlund et al. (2006) *Am. Min.*, 91, 295-305. [9]Fei (1999) *Am. Min.*, 54, 272-276. [10]Matsui et al. (2000) *Am. Min.*, 85, 312-316. [11]Nishiyama et al. (2004) *Phys. Earth Planet. Int.*, 143-144, 185-199. [12]Leinenweber et al. (2006) COMPRES Report. [13]Trønnes and Frost (2002) *Earth Planet. Sci. Lett.*, 197, 117-131.

Acknowledgements: Norimasa Nishiyama at GSECARS provided many hours of expert help at the beamline. Sophie Berthet and Valerie Malanergne provided assistance in experiment preparation. Powdered Allende sample was provided by the Smithsonian Institution.

ASTEROIDAL DIFFERENTIATION PROCESSES DEDUCED FROM ULTRAMAFIC ACHONDRITE UREILITE METEORITES.

Hilary Downes[1,2], David W Mittlefehldt[3], Pierre Hudon[4], Christopher S. Romanek[5] and Ian Franchi[6] [1]Lunar and Planetary Institute, Houston, Texas, USA (Downes@lpi.usra.edu); [2]School of Earth Sciences, Birkbeck, University of London, London, UK; [3]NASA/Johnson Space Centre, Houston, Texas, USA; [4]Dept. of Earth and Planetary Sciences, McGill University, Montreal, Quebec, Canada; [5] Savannah River Ecology Laboratory, University of Georgia, Aiken, SC, USA; [6]Planetary Sciences Research Institute, Open University, Milton Keynes, UK.

Introduction: Ureilites are the second largest achondrite group. They are ultramafic achondrites that have experienced igneous processing whilst retaining some degree of nebula-derived chemical heterogeneity [1, 2]. They differ from other achondrites in that they contain abundant carbon and their oxygen isotope compositions are very heterogeneous and similar to those of the carbonaceous chondrite anhydrous mineral line. Their carbonaceous nature and some compositional characteristics indicative of nebular origin suggest that they are primitive materials that form a link between nebular processes and early periods of planetesimal accretion. However, despite numerous studies, the exact origin of ureilites remains unclear. Current opinion is that they represent the residual mantle of an asteroid that underwent silicate and Fe-Ni-S partial melting and melt removal. Recent studies of short-lived chronometers [3,4] indicate that the parent asteroid of the ureilites differentiated very early in the history of the Solar System. Therefore, they contain important information about processes that formed small rocky planetesimals in the early Solar System. In effect, they form a bridge between nebula processes and differentiation in small planetesimals prior to accretion into larger planets and so a correct interpretation of ureilite petrogenesis is essential for understanding this critical step.

Sampling the ureilite parent asteroid: Polymict ureilites contain olivine and pyroxene clasts that cover an identical range of compositions to that shown by all known monomict ureilites [5,6], indicating derivation from a single parent asteroid. Each thin-section of a polymict ureilite may contain hundreds of clasts of ureilitic material, and multiple thin-sections greatly increase the number of clasts available for analysis. Therefore the potential for studying the parent asteroid of ureilites is much greater if polymict samples are analysed. We have analysed over 500 mineral or lithic clasts from polymict ureilites in order to compare the distribution of mineral compositions within samples and to shed light on ureilite petrogenesis. Although the basaltic material formed by partial melting is largely missing from the present-day meteorite collection, numerous melt clasts are present within polymict ureilites, indicating that such material was present on the surface of the asteroid [7]. Furthermore, our study shows that many individual mineral clasts in polymict ureilites have identical compositions to the unusual olivine and pyroxene grains from the Hughes 009 augite-bearing ureilite, considered to have undergone interaction between melt and residue [8]. We have also done petrologic, bulk chemical and isotopic study of a suite of monomict ureilites.

Two types of ureilite: Our study has confirmed the observation that ureilitic olivine grains with mg#s < 85 are more common than those with mg# > 85 [9]. Recognition of the existence of two groups of ureilites (**Fig. 1**) may be of major significance. The ferroan group comprises a coherent suite of olivine compositions with a strong negative correlation between Fe and Mn, whereas the magnesian group shows much more scatter and possibly even a positive correlation. There are also differences between the two groups in bulk C and siderophile element contents of monomict ureilites (**Figs. 2, 3**). Note that while there are two distinct groups, the actual boundary criterion that distinguishes the groups is uncertain. The two groups merge at mg# 85 for olivine compositions (**Fig.1**), but mg# 83-84 works better for C and Ir (**Figs. 2, 3**). The two groups represent the products of contrasting processes or, more likely, the disruption of a single process by impact.

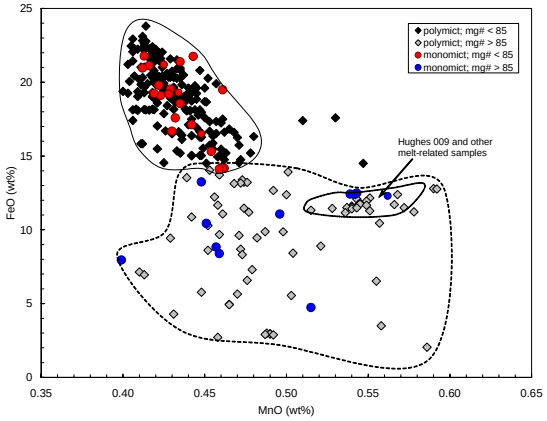

Figure 1. FeO vs MnO in ureilitic olivine grains from monomict ureilites and clasts within polymict ureilites. The coherent trend shown by samples with mg# < 85 is largely nebula-derived but overprinted by small degrees of melt extraction. Samples with mg#s > 85 were

undergoing partial melting at the instant of disruption of the parent ureilite asteroid.

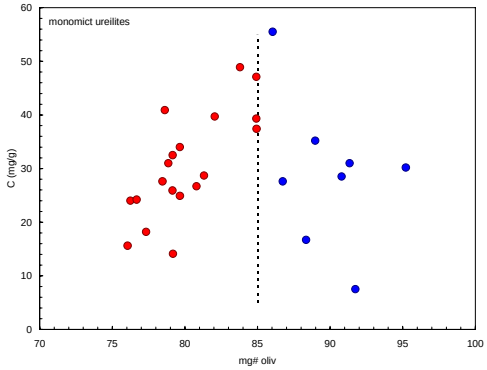

Figure 2. Bulk C vs olivine mg# in monomict ureilites. Samples with olivine mg# < 85 exhibit a positive correlation. Samples with olivine mg#s > 85 exhibit no coherent trend.

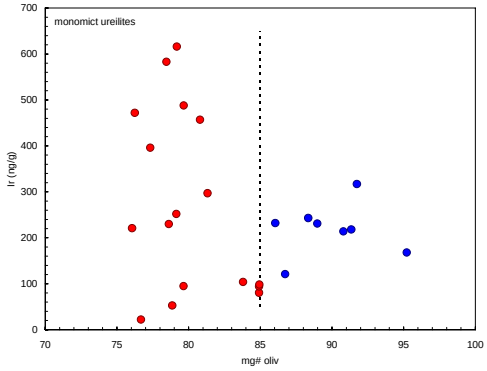

Figure 3. Bulk Ir vs olivine mg# in monomict ureilites. Samples with olivine mg# < 85 exhibit a wide range in Ir and no correlation. Samples with olivine mg#s > 85 have lower Ir contents on average, and possibly show a positive correlation.

Interpretation: We conclude that the proto-ureilite asteroid accreted from the solar nebula, probably as aggregates of olivine, orthopyroxene, diopside, plagioclase, metal, sulfide and carbonaceous material, with a range in mg# from ~74 to ~90 and wide $\Delta^{17}O$ variation. Ureilitic olivine compositions start abruptly at Fo74-75, the reason for which must relate to the minimum mg# of material in that part of the solar nebula from which the parent asteroid accreted. For comparison, the mantle of Mars also appears to have an mg# of ~75 [10]. The asteroid was heated by decay of radioactive ^{26}Al [11], causing metamorphism, and transformation of carbonaceous material to graphite. Siderophile contents of bulk ureilites indicate that removal of Fe-Ni-S melt may have occurred at this stage [12], perhaps forming a primitive core, but the high siderophile contents of some ureilites indicates that this process was incomplete (**Fig. 3**). As the inhomogeneous asteroid heated up, silicate melting would have commenced at the peritectic associated with the most iron-rich composition (mg# = 74-75), assuming a homogeneous Al distribution. Melting of each increment ceased when one (plagioclase) or more likely two (plagioclase + high-Ca pyroxene) of the original silicate phases had been consumed in the melting reaction and the melt expelled. This process explains the depletion of incompatible lithophile elements in ureilites [1]. It left behind a tri-mineralic olivine-pigeonite-graphite ureilite, essentially equivalent to a harzburgite in a more Mg-rich system (such as the Earth's mantle; mg# = 89). Thus the more abundant and more coherent group of ferroan ureilites probably represents residues from partial melting. However, this partial melting had occurred in a series of events in regions of the asteroid with different bulk mg#, so there was no planetesimal-wide magma ocean stage, and hence oxygen isotopes did not become homogenised. High precision oxygen isotope data for monomict ureilites can be interpreted as a series of small fractionation trends caused by partial melting [13].

One possible scenario is that the parent asteroid was disrupted by a major impact when melting reached silicate compositions with mg#s of approximately 85, giving rise to the two types of ureilites: (a) those that were already residual after melting and (b) those that were still partially molten when disruption occurred. In several samples with mg# > 85, melt impregnation of the mantle of the asteroid occurred, forming a suite of augite-bearing ureilites including Hughes 009 [8]. The impact event formed the highly shocked ureilite clasts found in polymict ureilites and represented in the monomict samples. It also formed the unusual highly magnesian rims around silicate minerals by a short-lived process akin to smelting. A daughter asteroid re-accreted from the remnants of the proto-ureilite asteroid; regolith formed on the daughter asteroid is represented by polymict ureilites. One problem with this scenario is that there is no quench-textured melt phase in mg# > 85 ureilites as might be expected from rapid cooling following disruption.

References: [1] Mittlefehldt D. W. *et al.* (1998) *Planetary Materials*, RIM 36, ch. 4. [2] Clayton R. N. and Mayeda T. K. (1988) *GCA* 52, 1313. [3] Goodrich C. *et al.* (2002) *MAPS* 37, A54. [4] Lee D.-C. *et al.* (2005) *LPSC* 36, #1638. [5] Goodrich C. A. *et al.* (2004) *Chemie der Erde* 64, 283. [6] Downes H. and Mittlefehldt D. W. (2006) *LPSC* 37, #1150.[7] Cohen B. *et al.* (2004) *GCA* 68, 4249. [8] Goodrich C. A. *et al.* (2001) *GCA* 65, 621. [9] Ikeda Y. *et al.* (2003) *Antarctic Meteorite Res.* 16, 105. [10] Dreibus G. and Wänke H. (1985) *Meteoritics* 20, 367. [11] Kita N. T. *et al.* (2003) *GCA Suppl.* 67, A220. [12] Warren P. *et al.* (2006) *GCA* 70, 2104. [13] Franchi I. A. *et al.* (1997) *MAPS* 32, A44.

THE VESTA – HED METEORITE CONNECTION. M. J. Drake, Lunar and Planetary Laboratory, University of Arizona, Tucson, AZ 85921-0092 (drake@lpl.Arizona.edu)

Introduction: There are two planets and one Moon from which we have samples. Earth and Moon have been sampled directly by humans. The connection of the Martian meteorites to Mars comes from young ages implying a relatively large planet, the match of noble gas patterns and isotopes in glasses in some Martian meteorites with the Martian atmosphere as measured by Viking, and by direct geochemical analysis of primitive basaltic rocks by instruments on the rover on the Mars Pathfinder mission [1-3]. Figure 1 shows the major element constraints.

Meteorites: Many lines of evidence indicate that meteorites are derived from the asteroid belt but, in general, identifying any meteorite class with a particular asteroid has not been possible. One exception is asteroid 4 Vesta, where a strong case can be made that it is the ultimate source of the howardite-eucrite-diogenite (HED) family of basaltic achondrites. Visible and near infrared reflectance spectra (Fig. 2) first pointed to a connection between Vesta and the basaltic achondrites [4]. Experimental petrology demonstrated that the eucrites (the relatively unaltered and unmixed basaltic achondrites) were the product of approximately a 10% melts [5]. Studies of siderophile element partitioning suggested that this melt was the residue of an asteroidal-scale magma ocean [6]. Mass balance considerations point to a parent body that had its surface excavated, but remains intact [7]. Modern telescopic spectroscopy has identified kilometer-scale "Vestoids" between Vesta and the 3:1 orbit-orbit resonance with Jupiter [8]. Dynamical simulations of impact into Vesta demonstrate the plausibility of ejecting relatively unshocked material at velocities consistent with these astronomical observations [9]. Hubble Space Telescope images (Fig. 3) show a 460 km diameter impact basin at the south pole of Vesta [10]. Spectroscopic studies of near-Earth asteroids revealed three small objects with basaltic composition which are arguably the proximal source of the HED meteorites, having reached one of Jupiter's resonances faster than the objects observed by [10] after which they quickly evolved into Mars crossing objects and then near-Earth objects. [11].

Conclusions: It seems that Nature has provided multiple free sample return missions to a unique asteroid. There is a conveyor belt of objects ejected from Vesta's surface stretching from Vesta to the 3:1 orbit-orbit resonance and into near-Earth space, with the near-Earth "Vestoids" being the proximal source of the HED meteorites.

References: [1] McSween H.Y, and Stolper E.M. (1980) *Sci. Am. 242, 54-63.* [2] Becker R.H. and Pepin R.O (1984) *Earth Planet. Sci. Lett. 69, 225-242.* [3] Drake M.J. and Righter K. (2002) *Nature 416*, 39-44. [4] McCord T. et al. (1970) *Science 168, 1445-1447.* [5] Stolper E.M. (1975) *Nature 258, 220-222.* [6] Righter K. and Drake M.J. (1997) *MAPS 32, 929-944.* [7] Consolmagno G. and Drake M.J. (1977) *Geochim. Cosmochim. Acta 41, 1271-1282.* [8] Binzel R.P. and Xu S. (1993) *Science 260, 186-191.* [9] Asphaug E. (1997) *MAPS 32, 965-980.* [10] Thomas et al. (1997) *Science 277, 1492-1495.* [11] Cruikshank et al. (1991) *Icarus 89, 1-13.*

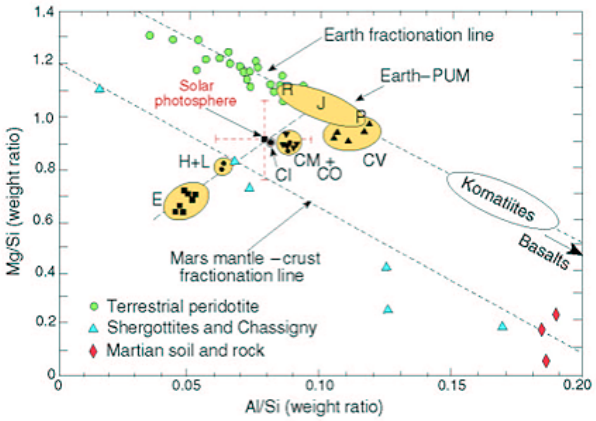

Figure 1. Mg/Si vs. Al/Si in primitive meteorites and Earth and Mars [3]. Note that Earth and Mars have distinct arrays implying different bulk compositions.

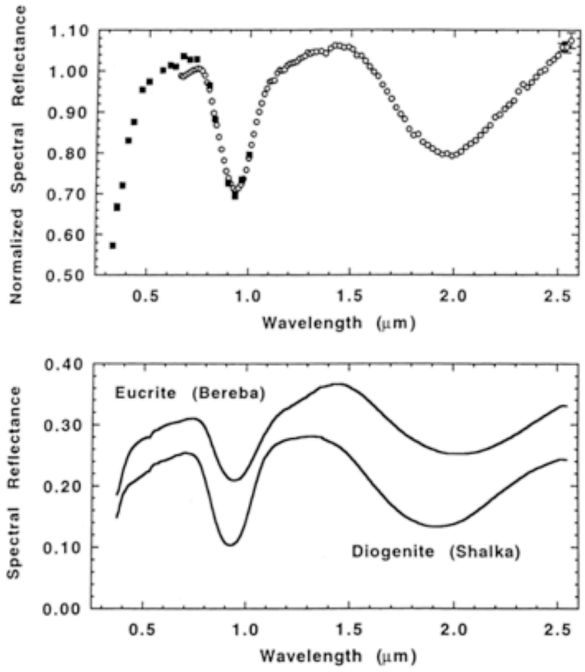

Figure 2. Modern reflectance spectra of Vesta (top panel) and eucrites (bottom panel) confirm the results of [4].

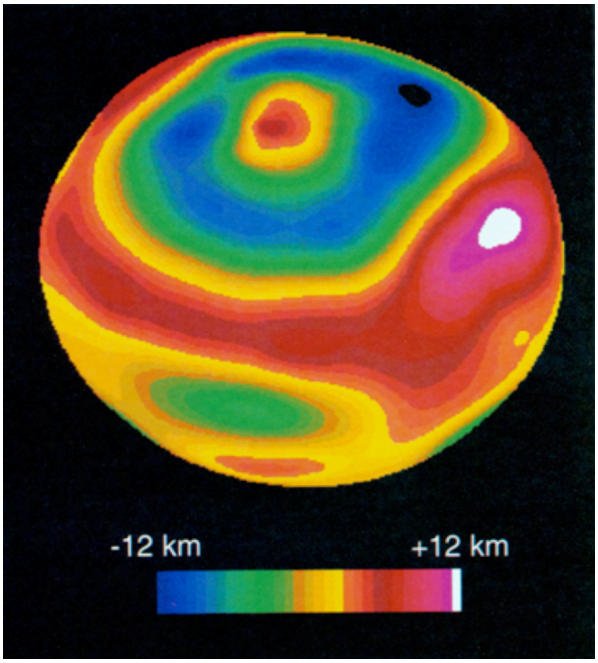

Figure 3. Hubble Space Telescope images of Vesta [[10]. Note that south is up in this image. A large crater surrounds the south pole.

POSSIBLE CORRELATION FOR PLANETARY FORMATION, BETWEEN GENERATION OF IMPACT CRATERS AND BOTH ACCRETION AND INITIAL CONDITIONS OF TERRESTRIAL PLANETS: NUMERICAL SIMULATION AND APPLICATION TO THE CAMPO DEL CIELO CRATER FIELD, SOUTH AMERICA. J. C. Echaurren, Codelco Chile Chuquicamata – North Division, jecha001@codelco.cl

Introduction: The initial conditions in the formation of terrestrial planets, might be correlated with the alterations generated seconds after of an impact with an asteroid or rock pieces. The produced heat by the impact energy, the melted matter, ejected pieces and dust in the gaseous environment, create abrupt changes in the chemical composition of both soil and atmosphere [1] on planets or stars, which change besides the direction evolutionary of a planet or star in development, in where the melted matter is accumulated as additional external material. These mechanisms on a large scale might influence powerfully in the formation and accretion of mass of giant planets as both Jupiter and Saturn [2], through the great heat liberated in massive impacts, that might accelerate the processes of accretion. An example of numerical calculation will be showed here, for the obtention of possible correlated conditions with initial conditions of terrestrial planets. The Campo del Cielo crater field located in Argentina (S27º 35', W61º 40'), is a possible example inside of the processes associated to the terrestrial formation. It contains at least 20 small craters, being the largest of them the crater Nº 3, with a diameter of ~ 103 m [3]. The crater field covers a 19 km x 3 km area and the craters were formed by fragments of an IA-type meteorite about 4000 years ago [3]. The mathematical model used here, is applied initially to the crater Nº 3, in quantum formalism, polynomial elements and Korteweg-DeVries (KDV) soliton theory [4], using a HP 49g, which is a Scientific Programmable Graphing Calculator with 1.5 Mb in RAM memory, other craters will be studied in future works. Then, for both, the impact event and calculations are used the diameter of crater Nº 3, elliptical shape and basement composition ~ clay.

Analytical Method and Results: According this model [4], the diameter of this piece of asteroid is ~ 3.34 m, with a velocity and impact angle of ~ 17.78 km/s and 9.91º respectively. The number of rings are calculated in ~ 0.1 with a initial crater profundity of ~ 14.46 m, this quantity could be altered across the passage of time from ~ 7.66 m to ~ 2 m, the melt volume is ~ 55.990E3 m^3 or ~5.70E –5 km^3 (~ 0.000057 km^3). The number of ejected fragments are estimated in ~ 170.9 with average sizes of ~ 0.67 m, and a cloud of dust with diameter of ~ 1.24 km. The total energy in the impact is calculated in ~ 3.27E21 Ergs, i.e., ~ 77.8 kilotons. Before of the erosion effects the transient crater is estimated in ~ 33.9 m, the hydrothermal zone (hydrothermal systems) is of ~ 4.85 cm to 16.97 m from the nucleus of impact. The lifetimes estimated for this hydrothermal zone are of ~ 561 years to ~ 876 years with uncertainties of ~ +/– 1.17 % to +/– 3.07 %, i.e., from +/– 6.56 years to +/– 26.92 years. Hydrothermal temperatures from 0.25 years to 1,400 years are estimated in ~ 670.7ºC to 22.29ºC respectively. The fragments are ejected to ~ 895 m from the impact center, with a velocity of ejection of ~ 767 m/s, ejection angle of ~ 0.43º and maximum height of ~ 1.67 m. The density of this piece of asteroid is calculated in ~ 7.14 g/cm^3, i.e., approximately a 90.76 % of Fe, according to this information is possible to calculate the mass in repose of this fragment in ~ 139.3 tons. The seismic shock-wave magnitude is calculated using linear interpolation in ~ 5.48 in the Richter scale. The maximum time of permanency for the cloud of both dust and acid in the atmosphere is ~ 10.07 hours and 2.1 days, respectively. The temperature peak in the impact is calculated in ~ 747,603 ºC, by a space of time of ~ 0.05 ms. The pressure in the rim of crater is calculated in ~ 2.17 Gpa. These results show the great variety of abrupt changes generated in the planetary environment, when a small piece of asteroid impacts the terrestrial surface. A high percentage of aspects relationed with accretion and initial conditions of terrestrial planets, are correlated with the phenomenon of impact craters generated by asteroids or pieces of them. Future works will be prepared in this area, looking for more precise correlations that relate both processes.

References: [1] Bond J. C. and Lauretta D. S. (2006). Chemical models of the protoplanetary disks for extrasolar planetary systems, *37th Annual Lunar and Planetary Science Conference*, March 13-17, Texas, USA, abstract Nº 1857. [2] Coradini, A. and Magni, G. (2006). Jupiter and Saturn evolution by gas accretion onto a solid core, *37th Annual Lunar and Planetary Science Conference*, March 13-17, Texas, USA, abstract Nº 1591. [3] Paillou P., Barkooky A. E., Barakat A., Malezieux J., Reynard B., Dejax J. and Heggy E. (2004). Discovery of the largest impact crater field on Earth in the Gilf Kebir region, Egypt, *C. R. Geoscience, 336*, 1491–1500. [4] Echaurren J. C. and Ocampo A. C. (2003). Model for prediction of potential hydrothermal zones on Isidis Planitia, Mars, *Geophysical Research Abstracts, Vol. 5*, 04450. *EGS-AGU-EUG Joint Assembly*, Nice, France.

THE FORMATION AGE OF KREEP BASED ON THE ^{147}Sm-^{143}Nd GEOCHEMISTRY OF KREEP-RICH ROCKS: DURATION OF LUNAR MAGMA OCEAN CRYSTALLIZATION AND SIMILARITY TO EARLY MARS.

J. Edmunson[1] and L. E. Borg[2], [1]Institute of Meteoritics, University of New Mexico (MSC03 2050, 1 University of New Mexico, Albuquerque, NM 87131-0001, edmunson@unm.edu), [2]Lawrence Livermore National Laboratory (7000 East Avenue, Livermore, CA 94550).

Introduction: Numerous ages for the solidification of the Lunar Magma Ocean (LMO) have been proposed using various radiogenic isotope systems. The ^{182}Hf-^{182}W age by [1] indicates that the LMO solidified 4527 ± 10 Ma ago. A ^{87}Rb-^{87}Sr age for the formation of KREEP (potassium, rare earth elements (REE), and phosphorous), the incompatible element-rich material formed during the last phase of LMO solidification from extreme (≥ 99.5%) fractional crystallization, is 4420 ± 70 Ma, assuming an initial Sm/Rb ratio of 2.3 [2,3]. The ^{146}Sm-^{142}Nd age for KREEP formation is 4320^{+56}_{-40} Ma [4,5]. Here, we present an additional age for the formation of KREEP and the solidification of the LMO using the ^{147}Sm-^{143}Nd isotopic system. The values calculated here for KREEP formation age and source ^{147}Sm/^{144}Nd ratios are compared to those calculated for Mars.

Observations: The REE signature that defines KREEP is found in Mg-suite samples, KREEP basalts, Apollo 14 pyroclastic glasses, and olivine gabbro cumulate meteorite North West Africa (NWA) 773. The petrogenetic relationships among these different KREEP lithologies are discussed by [6,7,8,9,10].

Magnesium-suite norite 78238 and KREEP-rich olivine gabbro cumulate NWA 773 were both analyzed at the University of New Mexico Radiogenic Isotope Laboratory. Norite 78238 has a ^{147}Sm-^{143}Nd age of 4334 ± 37 Ma and an initial ε_{Nd}^{143} value of -0.27 ± 0.74. The NWA 773 meteorite has a ^{147}Sm-^{143}Nd age of 3032 ± 32 Ma and an initial ε_{Nd}^{143} value of -3.51 ± 0.27 [11]. These two samples bracket the Mg-suite samples and KREEP basalts that have negative initial ε_{Nd}^{143} values in a time versus initial ε_{Nd}^{143} diagram (Fig. 1). The evolution line drawn through these KREEP-rich samples indicates that they were derived from sources with a ^{147}Sm/^{144}Nd ratio of 0.178 ± 0.006. The ^{147}Sm/^{144}Nd ratio presented here for KREEP-rich source regions is within error of the estimate of 0.181 by [12]. The observation that the source regions of these KREEP-rich samples have similar ^{147}Sm/^{144}Nd ratios suggests that they share a common origin, and that the KREEP component present in these samples formed by a similar extent of fractional crystallization of the bulk Moon. Note however that a KREEP component will dominate the REE signatures of individual source regions. Consequently, the fact that these KREEP-rich samples appear to be derived from sources with a common ^{147}Sm/^{144}Nd ratio does not imply that the sources are identical [7,9].

Comparison of lunar differentiation ages: A ^{147}Sm-^{143}Nd model age for KREEP formation, and hence the termination of silicate differentiation on the Moon, is defined by the intersection of the ^{147}Sm/^{144}Nd = 0.178 evolution line with the Chondritic Uniform Reservoir (CHUR) evolution line on Fig. 1. The resulting model age is 4492 ± 61 Ma. This age is within uncertainty of both the ^{182}Hf-^{182}W age for lunar differentiation by [1] and the ^{87}Rb-^{87}Sr age determined for KREEP formation by [2]. However, the ^{147}Sm-^{143}Nd age presented here is not within uncertainty of the age estimated for lunar silicate differentiation by the ^{146}Sm-^{142}Nd isotopic system [4,5].

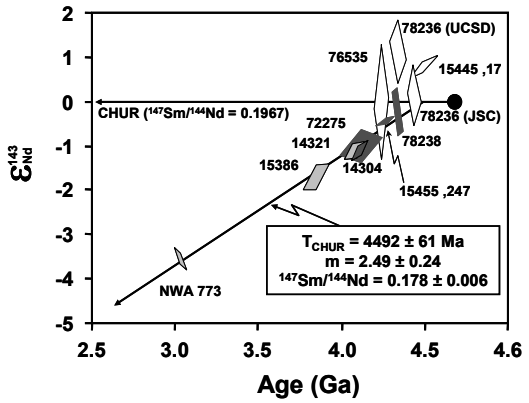

Figure 1: Time versus initial ε_{Nd}^{143} value diagram, illustrating the relationship between KREEP-rich samples [11]. Black circle = chondritic starting composition at 4558 Ma, white polygons = Mg-suite samples with positive ε_{Nd}^{143} values, dark gray polygons = Mg-suite samples with negative ε_{Nd}^{143} values, light gray polygons = KREEP basalts and KREEP-rich olivine gabbro cumulate NWA 773. The line regressed through the KREEP-rich samples with negative ε_{Nd}^{143} values indicates a common fractionation history for the KREEP signature of these rocks from source regions with a ^{147}Sm/^{144}Nd ratio of 0.178 ± 0.006. All data in this diagram has been renormalized to a La Jolla Nd standard value of 0.511850.

Comparison to Mars: The ^{147}Sm-^{143}Nd isotopic systematics of KREEP-rich samples share several characteristics with rocks derived from LREE-enriched sources on Mars. For example, the KREEP model age of 4492 ± 61 Ma is concordant with the ε_{Nd}^{142} - ε_{Nd}^{143} model age of 4525^{+19}_{-21} Ma suggested for martian silicate differentiation [e.g., 13]. Additionally, similar ^{147}Sm/^{144}Nd ratios calculated for lunar KREEP (0.178) and "martian KREEP" (0.182) from [14] suggest similar processes may be involved in producing each of these evolved, incompatible element-rich components. If the evolved component in both the Moon and Mars represents a late-stage liquid derived by crystallization of a magma ocean, the similar ^{147}Sm/^{144}Nd ratios of the source regions may indicate both lunar and martian magma oceans had similar evolutionary histories.

Discussion: One observation that must be resolved before the evolutionary histories of the Moon and Mars can be directly equated is the apparent discrepancy between the ^{146}Sm-^{142}Nd and ^{147}Sm-^{143}Nd ages of silicate differentiation on the Moon. The differentiation ages obtained by [4,5] using the ^{146}Sm-^{142}Nd system are significantly younger than the ^{182}Hf-^{182}W age from [1] and the ^{147}Sm-^{143}Nd age presented here, and only slightly within uncertainty of the ^{87}Rb-^{87}Sr age from [2]. Additionally, both the martian Sm-Nd systems appear to be concordant, with the ε_{Nd}^{142} and ε_{Nd}^{143} values yielding a combined age of 4525^{+19}_{-21} Ma for silicate differentiation [13]. The ε_{Nd}^{142} and ε_{Nd}^{143} values obtained for lunar samples, using the same approach, yielded two different ages for high-Ti mare basalts, and low-Ti mare basalts and KREEP-rich rocks combined [10]. Thus, the ^{146}Sm-^{142}Nd isotopic systematics of lunar samples do not indicate a single differentiation event.

Present-day ε_{Nd}^{142} values were calculated for mare basalts and KREEP-rich samples from [4,15] for comparison with the measured ε_{Nd}^{142} values. The model assumes a two-stage evolution in which growth is initially chondritic until the age of source formation at 4527 Ma. This age corresponds to the age of lunar differentiation based on the ^{182}Hf-^{182}W system [1]. The source regions were assumed to have the same ^{147}Sm/^{144}Nd ratios as the individual whole rocks that were modeled. On average, the measured ε_{Nd}^{142} values of the high-Ti mare basalts, the low-Ti mare basalts, very low-Ti basalt A881757, and ilmenite basalt 12056 were 0.53, 0.20, 1.13, and 0.77 ε_{Nd}^{142} units lower than predicted by the model. In contrast, KREEP-rich rocks were approximately 0.20 ε_{Nd}^{142} units too high. Thus, lunar rocks tend to have more muted ε_{Nd}^{142} values than expected (i.e., ε_{Nd}^{142} values closer to each other than what geochemistry predicts).

These observations imply that the ^{146}Sm-^{142}Nd system does not record the age of LMO solidification, but rather is disturbed by events occurring after the Moon solidified [1,4,15]. One possible reason for the younger differentiation age of the ^{146}Sm-^{142}Nd isotopic system is cumulate overturn and the resulting re-equilibration of the isotopic signature of the source region [15]. Alternatively, it could represent modifications to the ^{146}Sm-^{142}Nd isotopic system by secondary processes after the basalts formed. This could be related to impacts, or the effects of neutron fluence [1,4,15]. A third possibility is that the old ages for lunar differentiation recorded by the ^{182}Hf-^{182}W and ^{147}Sm-^{143}Nd isotopic systems may be incorrect.

Conclusions: The formation age of KREEP, and the solidification age of the LMO, is 4492 ± 61 Ma and is derived from the ^{147}Sm-^{143}Nd isotopic systematics of multiple lunar samples. This age was produced from a linear array of KREEP-rich samples in a time versus initial ε_{Nd}^{143} diagram. This linear array indicates that the KREEP-rich rocks were derived from sources with ^{147}Sm/^{144}Nd ratios of 0.178 ± 0.006. The fact that lunar KREEP has a calculated ^{147}Sm/^{144}Nd ratio within error of the calculated "martian KREEP" ^{147}Sm/^{144}Nd ratio indicates that both the lunar and martian magma oceans may have had similar, but not identical, evolutionary histories. One difference in their evolutionary histories is the potential post-differentiation disturbance of the ^{146}Sm-^{142}Nd isotopic system on the Moon.

References: [1] Kleine T. et al. (2005) *Science, 310*, 1671-1674. [2] Nyquist L. E. and Shih C. –Y. (1992) *GCA, 56*, 2213-2234. [3] Snyder G. A. et al. (1992) *GCA, 56*, 3809-3823. [4] Nyquist L. E. et al. (1995) *GCA, 59*, 2817-2837. [5] Rankenburg K. et al. (2006) *LPS XXXVII*, Abstract #1348. [6] Warren P. H. (1985) *Ann. Rev. Earth Planet. Sci., 13*, 201-240. [7] Borg L. E. et al. (2004) *Nature, 432*, 209-211. [8] Shearer C. K. et al. (2006) *In: New Views of the Moon*, eds. Jolliff, Wieczorek, Shearer, and Neal, 365-518. [9] Shearer C. K. and Papike J. J. (2005) *GCA, 69*, 3445-3461. [10] Shearer C. K. and Borg L. E. (2006) *Chemie der Erde Geochem., 66*, 163-185. [11] Borg L. E. et al. (2005) *LPS XXXVI*, Abstract #1026. [12] Nyquist et al. (2002) *LPS XXXIII*, Abstract #1289. [13] Foley C. N. et al. (2005) *GCA, 69*, 4557-4571. [14] Borg L. E. and Draper D. S. (2003) *M&PS, 38*, 1713-1731. [15] Borg L. E. and Wadhwa M. (2006) *LPS XXXVII*, Abstract #1154.

LINKED MAGMA OCEAN SOLIDIFICATION AND ATMOSPHERIC GROWTH: THE TIME FROM ACCRETION TO CLEMENT CONDITIONS. L.T. Elkins-Tanton and E. M. Parmentier, Brown University Department of Geological Sciences, Providence RI, USA (Lindy@brown.edu).

Introduction: For the purposes of calculating the cooling rate of a magma ocean and the time to solidification of a planet, the most important gases entering the early atmosphere are water and carbon dioxide. These two components, both relatively common in the potential planetary disk building blocks of Mars, are strong greenhouse gases and will significantly slow planetary cooling and retain a high temperature at the surface of the magma ocean. The importance of an early water atmosphere has been recognized and studied by Abe and Matsui [1] and Matsui and Abe [2] and further explored by Elkins-Tanton and Parmentier [3]. Here we add carbon dioxide to the calculations of magma ocean solidification and atmospheric growth.

Models: During magma ocean solidification elements are partitioned between the crystallizing minerals and the remaining, evolving magma ocean liquid. Nominally anhydrous minerals can contain a dynamically and petrologically significant amount of OH [4-8] (as much as 1000 ppm, and with contributions from minimal interstitial liquids, resulting mantle solids can retain 0.25 to 0.5 wt% H_2O [3]). Carbon dioxide, in contrast, cannot partition into mantle minerals in as significant quantities [9]. At pressures and temperatures of magma ocean crystallization no hydrous or carbonate minerals will crystallize [10,11].

Volatiles are therefore enriched in evolving liquids and will degas into the atmosphere when convection transports liquid close enough to the surface that bubbles can form and rise before being carried down again. At the surface, the volatiles again partition between the atmosphere and the magma ocean liquids according to their equilibrium partial pressures. Both water and carbon dioxide can dissolve into silicate melts at quantities greater than 10 wt% at pressures above their degassing pressures [e.g. 12], though at a given pressure water will remain in silicate liquids in greater concentration than will carbon dioxide. Carbon dioxide and water saturation curves are taken from Papale [13]. Because convective velocities are sufficient to bring all the liquid in the magma ocean near the surface during each time step of these models, volatiles are removed from the liquid uniformly at each step to create a magma ocean liquid with volatile concentrations in equilibrium with the atmosphere.

The initial volatile content of Mars is unknown. An estimate can be obtained by assuming that all the volatiles that accrete to the protoplanet before it reaches a radius sufficient to drive impact energy above what is required for devolatilization, estimated by Safronov [14] as ~1,300 km. The materials that accreted to create Mars are also unknown. The highest chondritic volatile content occurs in C1 chondrites, which may contain as much as 3.5 wt% carbon and 20 wt% water [15]. Some C3 and OC chondrites, in contrast, may contain only 0.5 wt% carbon and 1 wt% water [15]. These end members give possible volatile contents for bulk Mars of 0.06 wt% CO_2 and 1.2 wt% H_2O, and 0.01 wt% CO_2 and 0.06 wt% H_2O, respectively. The atmosphere at the beginning of solidification is assumed to be in equilibrium with these bulk volatile contents.

Magma ocean fluid dynamics differ significantly from solid mantle dynamics, and are closely modeled by the dynamics of atmospheres, as noted by Solomatov [16]. Heat is transported from the interior to the surface by cold thermal plumes descending from the upper boundary layer, accompanied by more diffuse return flow of hotter material from the interior. Heat is transmitted conductively from the upper boundary layer into any existing early atmosphere, which in turn inhibits radiation into space by its level of emissivity, proceeding from the work of Priestley [17,18] and Abe and Matsui [1]. Heat flux F from the planet can be expressed as the following balance:

$$4\pi R^2 F = V\left[\rho H 4\pi r^2 + \rho C_p \frac{dT}{dr}\frac{4}{3}\pi\left(R^3 - r^3\right)\right] \quad (1)$$

expressed in terms of planetary radius R, velocity of solidification front V, solid density ρ, heat of fusion H, radial increment of solidification r, heat capacity C_p, and change in solid temperature dT (dependent upon solidus slope). Total heat flux F can be calculated as Stefan-Boltzmann radiation from the atmosphere:

$$F = \varepsilon\sigma\left(T^4 - T_\infty^4\right), \text{ and } \quad \varepsilon = 2\left[\frac{3P\left(\frac{\kappa_0 g}{3p_o}\right)^{\frac{1}{2}}}{2g} + 2\right]^{-1}, \quad (2,3)$$

where emissivity ε is a function of atmospheric pressure P, gravitational acceleration g, and opacity κ_o at pressure p_o [19,20]. By inserting equations (2) and (3) into equation (1), the rate of solidification for each radial increment can be calculated, and a total time from liquid to solid mantle summed. Processes of magma ocean solidification are discussed in [21, 22, 16] and the details of these models in [23].

Results: A simplified initial model predicts several important effects on planetary evolution. Solidification rates limited by radiative heat loss through the atmosphere may be very fast, with 90% by volume of the magma ocean solidifying in as little as 10,000 years (Fig. 1). In further models including convective heat transfer through the atmosphere, cooling may proceed even faster. Dreibus and Wanke [24] have suggested that oxidizing reactions with iron release only hydrogen into the atmosphere rather than water. If the atmospheric masses predicted in this model are too high for equilibrium with the buffering reaction Fe + H_2O = FeO + 2H, then cooling will be more rapid. Even the rates predicted in these models probably allow almost complete solidification before solid-state gravitationally-driven cumulate overturn.

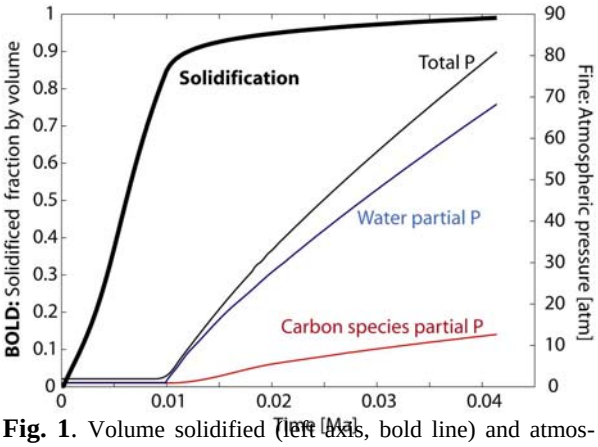

Fig. 1. Volume solidified (left axis, bold line) and atmospheric pressure (right axis, fine lines) for an initial magma ocean with 0.06 wt% water and 0.01 wt% carbon dioxide.

Though the great majority of volatiles remain in the evolving liquids or are degassed into the atmosphere, a geodynamically significant quantity is sequestered in the solid cumulates, as much as 0.03 wt% OH in even the driest models, without considering interstitial liquids. In the absence of plate tectonics, therefore, mantle volatile content should be controlled by magma ocean processes. Initial mantle water content has a significant effect on creep rates and thus mantle viscosity and onset and vigor of convection.

Carbon dioxide and water degas at different rates, creating an atmosphere with changing composition and emissivity. With small changes of initial composition the resulting early atmosphere can change from water-dominated to carbon dioxide-dominated (Fig. 2). The rapid cooling and high initial atmospheric pressures indicate that liquid water may have existed within a few million years of magma ocean solidification. Though Mars is relatively dry today, as much as 99% of Mars' original volatiles are thought to have been lost by 3.8 GPa through escape through impacts, sputtering by solar wind, and hydrodynamic escape [25].

Fig. 2. With small changes in initial magma ocean volatile compositions (indicated at top of each figure) the resulting atmosphere changes composition.

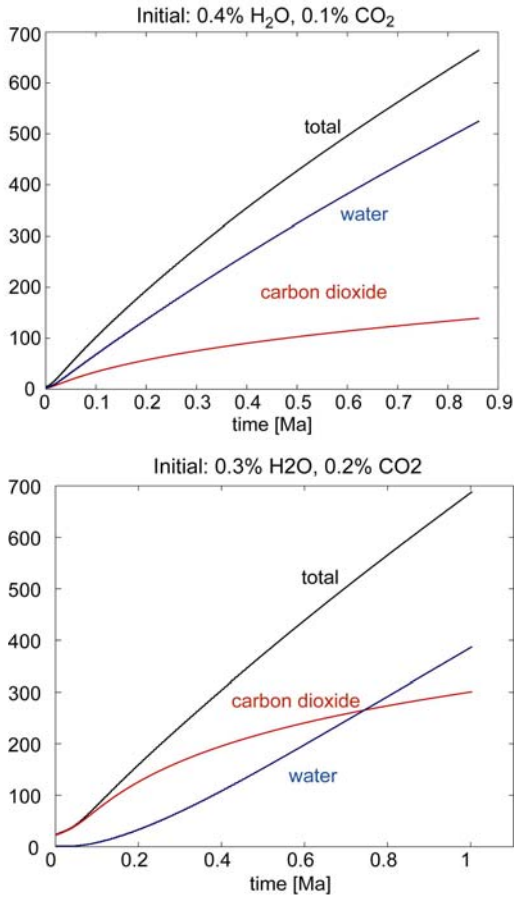

References: [1] Abe and Matsui (1988) *J. Atm. Sci 45*, 3081. [2] Matsui and Abe (1986) *Nature 319*, 303. [3] Elkins-Tanton and Parmenter (2005) LPS XXXVI. [4] Koga (2003) *G^3 4*. [5] Aubaud (2004) *GRL 31*. [6] Forneris (2003) *EPSL 214*, 187.[7] Bell (2004), *S. Africa J. Pet. 45*, 1539. [8] Bolfan-Casanova (2000) *EPSL 182*, 209. [9] Keppler (2003) *Nature 424*, 414. [10] Ohtani (2004) *PEPI, 143*, 255. [11] Wyllie and Ryabchikov (2000) *J. Pet. 41*, 1195. [12] Papale (1999) *Am. Min. 84*, 477. [13] Papale (1987) *CMP 126*, 237. [14] Safronov and Vitjazev (1986) *Chem. Phys. Terr. Planets* 1-29. [15] Wood (2005) *Chondrites and the Protoplanetary Disk*. [16] Solomatov (2000) *Origin Earth and Moon*, U. Ariz. [17] Priestley (1959) *Turbulent Transfer in Lower Atmosphere*, U. Chicago Press. [18] Priestley (1957) *Proc. R. Soc. London A238*, 287. [19] Pujol and North (2003) *Tellus 55A*, 328. [20] Hodges (2002) *GRL 29*. [21] Abe (1993) *Lithos 30*, 223. [22] Abe (1997) *PEPI 100*, 27. [23] Elkins-Tanton (2003) *MAPS, 38*, 1753. [24]Dreibus and Wanke (1987) *Icarus 71*, 225. [25] Catling (2004) Atmospheric Evolution of Mars. In: Gornitz (ed.) *Encyclopedia of Paleoclimatology and Ancient Environments.*

MARS VS. THE MOON: THE EFFECTS OF LENGTH SCALES AND INITIAL COMPOSITION ON PLANETARY DIFFERENTIATION. L. T. Elkins-Tanton, E. M. Parmentier, and P.C. Hess, Brown University, Department of Geological Sciences, 324 Brook St., Providence RI 02912, Lindy@brown.edu, EM_Parmentier@brown.edu.

Introduction: One or more magma oceans are hypothesized to have existed early in the evolution of the terrestrial planets, particular the Moon [e.g. 1-4]. The Moon is conspicuously marked by compositional differentiation in the form of its anorthosite highlands, while Mars, the Earth, and Venus appear to lack early plagioclase flotation. One of the most conspicuous features on Mars, in contrast, is its crustal dichotomy. These large-scale features that formed in the earliest stages of planetary evolution reasonably may be linked to the dynamic processes of planetary differentiation. First-order planetary characteristics such as radius and volatile content can be sufficiently influential to differentiation that they can produce end-members as different as the surface features of Mars and the Moon, even if both experienced deep magma oceans.

Models: Magma ocean solidification is calculated assuming that vigorous convection in the low viscosity liquid magma ocean maintains a homogeneous composition [5,6] and solidification proceeds from the bottom upward. Volatiles and other incompatible elements are enriched in the evolving magma ocean liquids as solidification proceeds. Subsequent cumulate overturn to gravitational stability is calculated using a thermochemical convection code.

Volatiles and Plagioclase Flotation: The Moon is likely a dry body formed from heated material following the giant impact with the Earth [7]. Its low mantle pressure range and dry magma ocean composition both encourage plagioclase formation. Mars was a wetter planet in its past, and its high mantle iron content indicates more oxidizing conditions during formation than were present on the Moon or even the Earth. Water in silicate melt suppresses plagioclase formation, and the higher pressure range of the Martian interior further limits its stability field. Water, then, may be one of the dominant variables in the outcome of magma ocean crystallization and subsequent planetary evolution.

On the Earth plagioclase may become stable at pressures from 1.5 to 0.9 GPa [*e.g.*, 8]. The depth of Mars at 1.5 GPa is 125 km, and corresponds to 90% solidification of a 2,000-km deep magma ocean. On the Moon, 1.5 GPa is reached at 360 km and represents 56% solidification of a 1,000-km deep lunar magma ocean. Solidification models of a Martian magma ocean beginning with 0.06 wt% water indicate that, when the pressure effects of an equilibrium atmosphere are included, the magma ocean liquids may contain 0.5 wt% water by the time the magma ocean is 90% solidified (Fig. 1). Experimental results show the plagioclase stability field is lowered by 70 to 100 degrees with the addition of 2 to 3 wt% of water [9, 10]. Plagioclase crystallization on Mars is therefore suppressed until late in solidification by both the planet's pressure gradient and by any water in the evolving liquids.

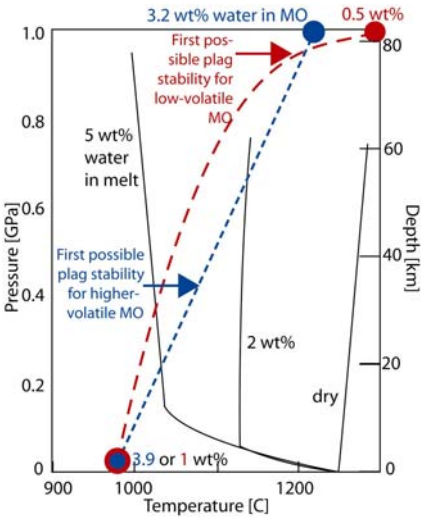

Figure 1: Possible evolved Martian MO liquids and the pressures of plag stability. *Solid lines*: Changes in plag stability in a Mt. Hood Andesite with addition of water [9]. *Long dashed line*: MO liquids from 0.06 wt% H_2O initial bulk composition. *Short dashed line*: Liquids with 1 wt% H_2O initial bulk composition. *Filled circles*: Points with labeled liquid water content. *Arrows*: Maximum pressure of plag crystallization from each MO composition.

Plagioclase flotation crust formation is therefore controlled by the magma's volatile content and the size of the body. Plagioclase flotation is also influenced by the magma density and therefore bulk Mg#: the molten enstatite chondrite parent body, for example, has a sufficiently high bulk Mg# that magma ocean liquids would not reach high density though iron enrichment. A similar situation may have prevailed on Mercury.

Plagioclase flotation may be one of the few ways to create a lasting crust on a liquid magma ocean (quench crusts will founder [10]). Such a crust, in the absence of an insulating atmosphere, will slow the cooling of the planet significantly. For this reason the Moon may have remained partially molten far longer than Mars, which likely cooled through convection with little or no conductive crust to slow heat transfer.

Depth of Magma Ocean and Initial Crustal Compositions: The timing of planetary accretion, radiodecay, and core formation, and the state of insulation of the planet, may have allowed heat to conduct into

planet, may have allowed heat to conduct into space sufficiently that only a portion of a terrestrial body's silicate mantle melted. Righter *et al.*[11] determined that Martian Ni, Co, Mo, W, P and Re abundances estimated from melt inclusions in Martian meteorites are consistent with a magma ocean of only 700 to 800 km depth. Rubie *et al.* [12] estimated the depth of a terrestrial magma ocean to be 550 km based on Ni partitioning.

Fractional crystallization from a magma ocean necessarily creates early cumulates with lower densities (higher MgO content) than the undifferentiated progenitor, and late cumulates from evolved liquids that are denser (higher FeO content) than any undifferentiated material. If viscosity is low enough to allow flow during solid-state cumulate overturn, the primitive material will rise to a level of neutral buoyancy in the Martian mantle, perhaps sufficiently to allow adiabatic melting.

On Mars, if the partial magma ocean is as deep as ~1,550 km (~ 19 GPa) then the layer of differentiated majorite + ringwoodite that crystallizes between 19 GPa and 14 GPa is thick enough to rise during gravitational overturn above its solidus and melt to produce an early basaltic crust. In a partial magma ocean between ~1,550 and ~1,250 km (~15 GPa) deep neither the primitive material nor the majorite + ringwoodite cumulates rise sufficiently to melt. The only magma produced for an early crust is from the shallowest pyroxene + olivine composition and is identical in composition to that created from the whole-mantle magma ocean. If, however, the magma ocean is less than ~1,150 km (~14 GPa) deep, the primitive material rises sufficiently during overturn to melt adiabatically. These experiments therefore indicate that different initial magma ocean depths will produce distinct compositions of earliest planetary crust, and will in some cases create two distinct compositions.

Planetary Radius and a Heterogeneous Mantle: Though in general the magma ocean cumulates increase in density with radius, solidification models indicate that cumulates do not form a monotonic density gradient: in all models cumulates in portions of the lower and upper mantle have identical densities but different bulk compositions and correspondingly different mineralogies.

Numerical experiments indicate that non-monotonic density profiles readily overturn to form mantles that are laterally heterogeneous compositionally [10, 13]. The final density structure after overturn is one where the radial density stratification decreases monotonically with radius. The densest materials from near the surface sink to the core-mantle boundary and buoyant mid-mantle material rises to the surface. Upgoing and downgoing plumes, however, stall at neutral buoyancy, creating a radius interval containing large-scale lateral heterogeneity in temperature, mantle composition and concentrations of radiogenic and trace elements. This lateral heterogeneity has implications for magmatic source regions as well as the initiation and pattern of thermal convection, and can be seen in temperature profiles in Fig. 2. The final overturned cumulate stratigraphy, therefore, is radial in its density structure but laterally heterogeneous in composition.

The smaller pressure range of the Moon produces a greater volume of cumulates with similar density than does a planet with a larger pressure range, like Mars. In a pure fractional crystallization model, following overturn to stability, the Moon has a laterally-heterogeneous mantle over 50% of its 1,000 km initial magma ocean depth. Mars, in comparison, has a laterally-heterogensous mantle over only 33% of its 2,000-km cumulate mantle (Fig. 2). One important effect of planetary radius on early differentiation that includes a magma ocean, then, is that smaller bodies will obtain far more heterogeneous mantles. On the Moon this result is consistent with the many compositions of picritic basalts that appear to have originated at similar depths. Critically, then following early differentiation no body will have a simple composition-depth relationship.

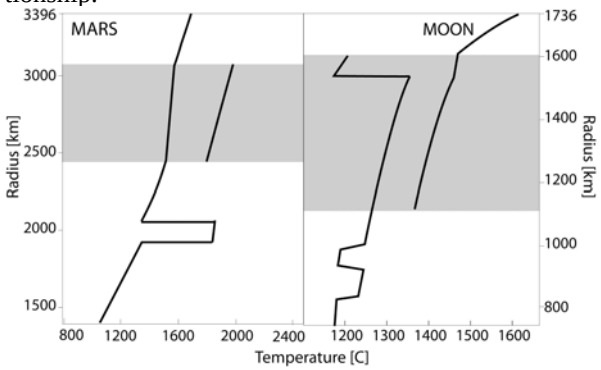

Figure 2: Mantle temperatures of Mars (left) and the Moon (right) following overturn of the cumulate mantle to gravitational stability. The shaded regions indicate the depth ranges over which the mantle is laterally heterogeneous in composition and temperature.

References: [1] Wood *et al.* (1970) Proc. Apollo 11 LPSC, 965-988. [2] Smith *et al.* (1970) Proc. Apollo 11 LPSC, 897-925. [3] Warren (1985) *Ann. Rev. Earth Planet. Sci. 13*, 201-240. [4] Tonks and Melosh (1993) *JGR 98*, 5319-5333. [5] Solomatov (2000) *Origin Earth and Moon*, U. Ariz.. [6] Elkins-Tanton *et al.* (2003) *MAPS, 38*, 1753-1771. [7] Hartman and Davis (1975) *Icarus 24*, 504-515. [8] Presnall *et al.* (2002) GCA 66, 2073-2090. [9] Johnson *et al.* (1994) Rev. in Mineralogy 30, 281-330. [10] Elkins-Tanton et al. (2005) *JGR* doi:10.1029/2005JE002480, 2005. [11] Righter *et al.* (1998) *GCA 62*, 2167-2177. [12] Rubie *et al.* (2003) EPSL 205, 239-255. [13] Zaranek and Parmentier (2004) JGR doi: 10.1029/2003JB002462.

MID-IR SPECTROSCOPY OF M ASTEROIDS WITH THE SPITZER SPACE TELESCOPE: HOW MANY ARE REALLY DIFFERENTIATED CORES? J. P. Emery[1], L. F. Lim[2], T.H. McConnochie[3], [1]*SETI Institute / NASA Ames (jemery@mail.arc.nasa.gov),* [2]*NASA/Goddard Space Flight Center (lucy.f.lim@nasa.gov),* [3]*Cornell University (mcconnoc@astro.cornell.edu).*

Introduction: We are conducting a survey of the emission spectra of 27 class M asteroids using the Infrared Spectrgraph (IRS; 5.2–38 μm) on the Spitzer Space Telescope. Although the visible and near-IR spectra of these asteroids are nearly featureless, ten of them are now known to have hydration features at 3 μm that are absent in the spectra of 15 others [1]. High S/N spectroscopy of these asteroids in the mid-IR is likely to reveal key thermophysical and compositional information not available in the near-IR.

The Masteroid taxon as originally designated [2, 3] comprised asteroids of moderate albedo that lacked mineral absorption features in the visible and near-IR (0.3–1.1 μm). In the absence of direct spectral evidence of composition, the nature of M asteroids has remained uncertain. In one interpretation [e.g. 4] they are considered to be the asteroid analogues to nickel-iron meteorites, in which case they would be fragments of the cores of one or more parent bodies which must have undergone extensive igneous differentiation before being catastrophically disrupted. Alternatively [5] they have been seen as analogues of the highly reduced enstatite ("E") chondrites, whose parent bodies could not have been differentiated or indeed melted at all.

Previous Evidence for Metallic and NonMetallic M-Asteroids: Radar observations have provided the most compelling direct evidence for the metallic compositions of at least some M asteroids. Very high radar albedos [6, 7] have been observed for various M asteroids, including 16 Psyche, 216 Kleopatra, and several near-Earth objects, consistent with high metal concentrations. The existence of nickel-iron meteorites also implies that their parent bodies must be somewhere among the small bodies of the Solar System. Laboratory studies of iron meteorites [8] suggest that at least 70 distinct metallic parent bodies are represented in the meteorite collection.

Radar observations of at least one other M asteroid [21 Lutetia; 9] suggest that its composition is nonmetallic. A nonmetallic nature for 21 Lutetia and various other M asteroids is also supported by observations of 3-μm absorptions which are characteristic of hydrated silicate minerals. These were first detected in the spectra of the M asteroids 55 Pandora and 92 Undina by Jones *et al.* [10]. These findings were confirmed by Rivkin *et al.* [1, 11], who surveyed the 3-μm spectra of 27 M asteroids and found hydration features on Pandora, Undina, Lutetia, and seven others. On the basis of these observations, they suggested that the former "M" class should be divided into "M" asteroids, which lack hydration features, and "W" asteroids, which resemble the "M" in the visible and near-infrared but are in fact hydrated. The nonmetallic composition of another hydrated M-asteroid, 22 Kalliope, was supported by the findings of Margot and Brown [12], who discovered Kalliope's satellite and were thus able to determine that Kalliope's density was too low for a metallic composition to be plausible.

Target List: Our observing list includes 25 of the 27 asteroids previously observed at 3 μm by Rivkin *et al.* [1]. Six of these were also observed in the near-IR by Hardersen *et al.* [13], who detected weak low-iron pyroxene features in five of them, two of which had hydration features at 3 μm. We also include 69 Hesperia, in which pyroxenes were detected [13], and 325 Heidelberga, in which no near-IR silicate features have been detected. A major goal of this survey is to determine whether mid-IR silicate features, which unlike near-IR features should be sensitive to non-iron-bearing minerals, correlate either with the subcategories of M asteroids established by the hydration data [1] or the pyroxene data [13]. Moreover, if any of these M asteroids are asteroid analogues of the enstatite chondrites, which are about 45% enstatite by volume [e.g. 14] and essentially featureless in the near-IR, they should be easily recognizable in the Spitzer IRS data.

Preliminary Thermal Results: Spectra of 26 of the 27 asteroids in our program have now been acquired. IRS covers the spectral range 5.2–38 μm in four low-resolution (R~64-128) modules. Two high resolution (R~600) modules operate from 9.9–37 μm. All objects were observed with the short wavelength (SL; $\lambda < 14.2$ μm) modules. Fifteen of the objects in our program were too bright for the long-wavelength (LL; $\lambda > 14.2$ μm) low-resolution modules, so these were observed with the high-resolution mode (SH, LH). The SH module overlaps with the SL1 module from 9.9 to 14.2 μm, providing confimation of spectral features detected in this important region on the long wavelegth edge of the silicate resonance band near 10 μm.

Subsolar-point temperatures are derived by fitting the data with the asteroid standard thermal model ["STM"; e.g. 15], allowing the radius, albedo, and beaming parameter (η) to float. The radius and albedo

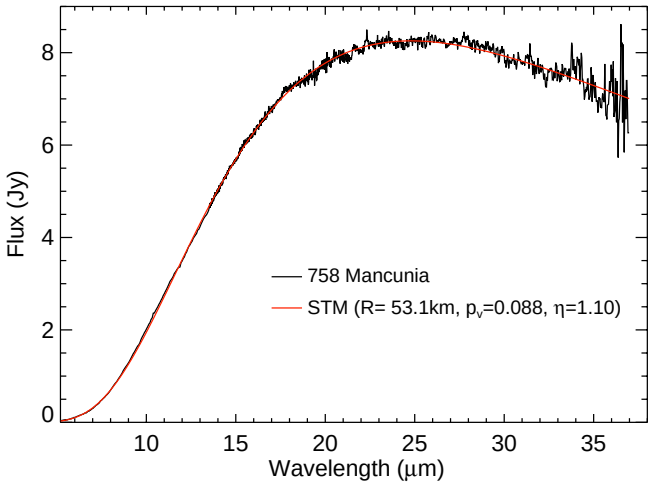

Figure 1. Thermal flux spectrum (black line) and best-fit thermal continuum model (STM; red line) for 758 Mancunia.

are additionally constrained by the visible absolute magntude (H_v). The results ofthese fits are illustrated in Figure 1 for 758 Mancunia. The veracity of the radiometric technique as we use it here is significantly improved over typical ground based mid-IR photometry by the broad and continuous spectral coverage afforded by Spitzer/IRS; coverage which includes the peak int he thermal emission. In the STM, the asteroid's thermophysical properties are summarized in a parameter η, which is related to the maximum (subsolar-point) temperature: $T_{ss}=[S(1-A)/(\eta\varepsilon\sigma)]^{1/4}$, where S is the insolation, A is the Bond albedo, and ε is the effective emissivity. The STM was originally calibrated using radii derived by stellar occultations. Large, Main Belt asteroids were found to have negligible thermal inertia and to be well described by an STM with η=0.756 ± 0.014 [15]. Higher η values, particularly η > 1, suggest an unusually high surface thermal conductivity.

During the model iterations to derive the best fit radius, albedo, and η, we calculate the visible geometric albedo (p_v) from the radius using the tabulated H_v for that object ($2R=1329*10^{-Hv/5}/\sqrt{p_v}$). The Bond albedo is then derived according to the formula $A=p_vq$, where q is the phase integral (typically ~0.39 for asteroids). Uncertainties in H_v do not significantly affect the radius determination, but do have direct bearing on the derivation of p_v. The largest source of uncertainty for most of the M asteroids is the lightcurve amplitude. If the IRS obserations were made at lightcurve maximum or minimum, then the derived albedo will be in error by an amount that depends on the light curve amplitude. Because η is effectively calculated from T_{ss} and the albedo, error in η are also related to errors in albedo. However, since $\eta \propto (1-p_vq)$, uncertainties in H_v and therefore p_v have only a small effect on η (few % at most).

The effective emissivity can also influence the derived beaming parameter. Silicate materials do not differ greatly from each other in effective emissivity, but a solid metal asteroid might have a much lower emissivity. Since η is inversely proportional to ε, a 10% decrease in ε will result in a 10% increase in η. We have assumed ε=0.9 (appropriate for silicates), but if some of these surfaces are truly metallic, then η will be higher than we derived.

Discussion: We will present results of thermal modeling of these data. Particular attention will be paid to whether thermal properties correlate with physical properties such as radar albedo, near-IR silicate bands, or 3-μm hydration bands. We will also present results of compositional analysis of emissivity spectra, which are derived by dividing the measured thermal flux spectrum by the best fit model thermal continuum. Strong Si-O vibrational bands in silicates near 10 and 20 μm offer a direct means to distinguish between silicate and metallic compositions.

References: [1] A. S. Rivkin, E. S. Howell, L. A. Lebofsky, B. E. Clark, D. T. Britt (2000) *Icarus* **145**, 351. [2] D. J. Tholen (1984) *Ph.D. Thesis*. [3] D. J. Tholen, *Asteroids II* (1989), pp. 1139–1150. [4] T. V. Johnson, F. P. Fanale (1973) J. Geophys. Res. **78**, 8507. [5] C. R. Chapman, J.W. Salisbury (1973) *Icarus* **19**, 507. [6] S. J. Ostro, D. B. Campbell, I. I. Shapiro (1985) *Science* **229**, 442. [7] D. L. Mitchell, *et al.* (1995) *Icarus* **118**, 105. [8] J. T. Wasson (1995) *Meteoritics* **30**, 595. [9] C. Magri, *et al.* (1999) *Icarus* **140**, 379. [10] T. D. Jones, L. A. Lebofsky, J. S. Lewis, M. S. Marley (1990) *Icarus* **88**, 172. [11] A. S. Rivkin, *et al.* (1995) *Icarus* **117**, 90. [12] J. L. Margot, M. E. Brown (2003) *Science* **300**, 1939. [13] P. S. Hardersen, M. J. Gaffey, P. A. Abell, (2005) *Icarus* **175**, 141. [14] A. Patzer, *et al.* (2004) *Meteoritics and Planetary Science* **39**, 1555. [15] L. A. Lebofsky, J. R. Spencer, *Asteroids II* (1989), pp. 128–147. [16] L. F. Lim, T. H. McConnochie, J. F. Bell, T. L. Hayward (2005) *Icarus* **173**, 385.